The Complex Chemical Abundances and Evolution of the Sagittarius Dwarf Spheroidal Galaxy[1]

Tammy A. Smecker-Hane[2]

Department of Physics & Astronomy, 4129 Frederick Reines Hall, University of California, Irvine, CA 92697–4575

tsmecker@uci.edu

and

Andrew McWilliam

The Observatories of the Carnegie Institute of Washington, 813 Santa Barbara St., Pasadena, CA 91101–1292

andy@ociw.edu

ABSTRACT

We report detailed chemical abundances for 14 red giant stars in the Sagittarius dwarf spheroidal galaxy (Sgr dSph), derived from echelle spectra obtained with the Keck I 10–meter Telescope. The stars span a wide range of metallicities, $-1.6 \leq$ [Fe/H] ≤ 0.0, with ages from $\sim$ 1 to 13 Gyr. At low metallicity, [Fe/H] < -1, the composition closely resembles the Galactic halo. However, for the metal-rich Sgr stars, with $-0.6 \leq$ [Fe/H] ≤ 0, the relationship of [α/Fe] with [Fe/H] is lower than that of the Galactic disk by 0.1 dex, while the light elements [Al/Fe] and [Na/Fe] are deficient by $\sim$ 0.4 dex. These ratios imply that 60 to 70% of the iron in the metal-rich population came from type Ia supernovae (SNe), and that type Ia produce some α elements but little or no sodium or aluminum. The neutron-capture heavy elements, as indicated by La and Eu, show an increasing s–process component with metallicity, up to [La/Fe] $\approx +1.0$ at [Fe/H] ≈ 0. The high ratio of heavy to light s–process elements, [La/Y] $\approx +0.5$, in the metal–rich population shows that their s–process enrichments came directly from AGB stars of the metal–poor population. Our abundances can be understood best if the Sgr dSph formed stars over many Gyr and lost a significant fraction of its gas during its evolution, such that ejecta from an aging metal-poor population dominated the metal–rich, star–forming gas. This gas was enriched with a higher ratio of type Ia/type II ejecta

[1]Data presented herein were obtained at the W.M. Keck Observatory, which is operated as a scientific partnership among the California Institute of Technology, the University of California and the National Aeronautics and Space Administration. The Observatory was made possible by the generous financial support of the W.M. Keck Foundation.

[2]Visiting Astronomer, Keck Observatory

than the solar neighborhood, implying that either the star–formation rate in the Sgr dSph underwent a lull or it operated with a longer e-folding time than that of the solar neighborhood. AGB stars from the metal-poor population produced large quantities of *s*-process elements with [La/Y] ratios characteristic of the low metal content. The steady increase in *s*-process elements relative to iron suggests that either iron production decreased or *s*-process efficiency increased with time. In addition, we discuss the insights this work gives us on whether or not mergers of dSph-like fragments were important in the evolution of the Galactic halo.

Subject headings: stars: abundances — galaxies: abundances — galaxies: evolution — galaxies: dwarf — galaxies: individual (Sgr dSph)

1. Introduction

The Sagittarius dwarf spheroidal galaxy (Sgr dSph) is currently being ripped apart and accreted onto the Milky Way (Ibata et al. 1997, and references therein). Tidal debris from the Sgr dSph appears to litter the Galactic halo tracing out Sgr's orbit (Dohm-Palmer et al. 2000, Newberg et al. 2002). How many and how frequently have mergers of dSphs affected the evolution of the Galaxy? When did they occur? We can answer these questions by determining the distributions of ages and chemical abundances in dSphs and comparing them with those of Galactic stars (Unavane, Wyse & Gilmore 1996, Mateo 1996, Shetrone, Côté, & Sargent 2001, Fulbright 2002). Abundance ratios, [X/Fe], of the intermediate–mass elements such as Na, Al, and the α elements, O, Mg, Si, Ca, Ti, provide powerful constraints on how much of the Galactic halo could have been formed in dSph–sized fragments because halo stars have [α/Fe] that is independent of metallicity and approximately equal to the theoretical average yield of type II SNe (except for Ti). (For reviews see Wheeler et al. 1989 and McWilliam 1997.) After a instantaneous burst of star formation, type II SNe quickly produce ejecta with high [α/Fe] on timescales of $\sim 10^7$ yrs, while type Ia SNe slowly produce ejecta with low [α/Fe] beginning at ~ 0.1 Gyr and continuing for many Gyr. Thus the Galactic halo has been inferred to have formed quickly because only ejecta from short–lived type II SNe, and **not** from long–lived type Ia SNe, were incorporated into most halo stars.

Contrary the rapid evolution of the Galactic halo, we now know that many of the Local Group dSphs have had surprisingly complex star–formation histories, despite their small mass (10^7 to $10^8 M_\odot$) and current lack of gas (see Smecker-Hane & McWilliam 1999, and Grebel 2000 for recent reviews). Color–magnitude diagrams show Sgr dSph stars have a wide range in age, $\sim$ 1 to 15 Gyr, and a wide range in metallicities from $-2 \leq$ [Fe/H] ≤ -0.7 (Bellazzini et al. 1999, Layden & Sarajedini 2000). Such complex evolution should leave obvious signatures in the abundance ratios of the stars (Gilmore & Wyse 1991). Will Sgr dSph stars contain a mix of Type Ia and II ejecta? Yes, if the dSph can recycle ejecta over long timescales as supported by the observed ranges in age and metallicity. No, if the first Type II SNe disrupt the interstellar medium in less than 0.1

Gyr and clear the way for subsequent SNe ejecta to escape in galactic winds, or if dSphs accrete fresh gas that fuels star formation at later times. Therefore, determining the abundance ratios in Sgr dSph stars also gives us unprecedented information on its evolution. The abundance ratios of the metal–poor stars can constrain the initial mass function of the massive stars that exploded as Type II SNe, which is critical for estimating the energy available to power galactic winds. By modeling the measured abundances as a function of metallicity or age, we can constrain the rate of enrichment from Type Ia and II SNe, star–formation rate, and the inflow/outflow of gas from the dSph.

We have obtained high–dispersion spectra of 14 red giants stars in the Sgr dSph and derived abundances for 24 elements. In this paper we report our results for Na, Al, α elements (Si, Ca, Ti), Fe and neutron capture elements (La, Y, Eu). In addition, we derive ages for the stars by comparing their inferred bolometric luminosities and effective temperatures to Padova stellar evolutionary models (Girardi et al. 2000). We conclude that star formation and chemical enrichment occurred over many Gyr in the Sgr dSph.

In a forthcoming paper, we will present data on the remaining elements, which include O, Mg, Sc, V, Cr, Mn, Co, Ni, Cu, Zr, Mo, Ba, Ce, Pr, and Nd.

2. The Sgr dSph Sample

Program stars were selected to span the full range in color of red giant branch stars in order to probe the full range of metallicities. Our sample was selected from the two fields near the center of the Sgr dSph imaged in VI–bands by Sarajedini & Layden (1995; hereafter SL95), and our stars were identified as members of the Sgr dSph based on radial velocities obtained from low–dispersion spectra by Ibata et al. (1997). We also obtained infrared JK–band photometry for the stars in our sample using the Cerro Tololo Inter-American Observatory 1.5–meter telescope. These data will be presented in a separate paper (Smecker-Hane, in preparation). The combined VIJK–band photometry was used to better quantify the effective temperatures of the stars. Table 1 presents the star list, coordinates, and photometry. The star ID numbers are listed as X–Y where X is the number of the SL95 field, where 1 denotes the M54 and Sgr field and 2 denotes the second Sgr field, and Y is the stellar ID number from SL95's photometry list. Note that M54 is a globular cluster that is a member of the Sgr dSph.

In Figure 1, we show the dereddened color–magnitude diagram (CMD) of the Sgr dSph based on the SL95 photometry, where we have assumed a reddening of E(V–I)= 0.18 and distance modulus of $(m - M)_V = 17.65$ as derived by SL95. The 14 stars in our spectroscopic sample are marked by large circles. In order to show a fairer representation of the field star population in the Sgr dSph, we have excluded stars that are within 2 arcmin of the center of the globular cluster M54. Readers should note that the sequence of stars located at $((V - I)_0, M_V) \approx (0.1, 0.75)$ is not the main-sequence turnoff of a young population; this sequence is the extended blue horizontal branch

of M54. However, more extensive photometry by Bellazzini et al. (1999) and Layden & Sarajedini (2000) in which they statistically subtract out the Galactic foreground shows that a young, metal–rich, population does exist (for example, see Bellazzini et al.'s Figure 11). Note that the color–magnitude diagram is heavily contaminated by Galactic foreground dwarfs because the Sgr fields lie at low Galactic latitude, $b = -14°$. The main sequence turnoff of the Galactic disk appears as a prominent vertical feature at $(V - I)_0 \approx 0.7$, and lower-mass main-sequence dwarfs become more prominent in the diagram at fainter magnitudes and redder colors. For reference, we have overplotted isochrones based on the Padova models (Girardi et al. 2000) for a variety of ages and metallicities.

3. Observations

High–dispersion spectra of 14 Sgr dSph red giant stars were acquired with the Keck I 10–meter telescope and the echelle spectrograph HIRES (Vogt et al. 1994) over 6 separate observing runs from 1996 to 1998. A total of 9 nights were allocated to this project. Bad conditions — clouds, high humidity, poor seeing, etc. — plagued our initial observing runs, and the study progressed slowly. In our first run, we split nights with another team so that we could maximize the amount of observing time on the Sgr dSph, a southern hemisphere object. Our second run was lost due to bad weather. Because of poor conditions, we obtained spectra of our initial 3 stars on our first and third runs. These spectra were reduced and analyzed separately, and the equivalent widths measured from the pairs of spectra were averaged before the final abundances were calculated.

The HIRES spectra were taken with the red collimator and the C5 decker, which has a slit width of 1.0 arcsec. The spectra have resolving power R $\sim$ 34,000, and the 22 orders that fall on the CCD cover a wavelength range of 5210 – 7650 Å. Note that gaps do occur in the wavelength coverage, because the CCD is not wide enough to capture the width of a full order. The seeing, as measured by the full width at half maximum of the stellar profile along the spatial direction, was an average of 1.0 arcsec, although it varied widely from 0.8 to 2.5 arcsec depending on observing conditions. The CCD had a pixel scale in the spatial dimension of 0.194 arcsec/pix, gain of 2.4 e^-/adu, and readnoise of 4.0 e^-.

Table 2 presents the details of the observations: star IDs, observing run, total exposure time, and the average signal-to-noise ratio per extracted pixel (SNR) in the combined spectrum determined by propagating the errors in the extraction and reduction process. The average exposure time per star was 2.5 hours, and the average SNR $\approx$ 55.

Multiple spectra (4 to 6) were taken of each star with individual exposure times being $\lesssim$ 30 mins so that the effect of cosmic rays could be mitigated in the data reduction. HIRES is a very stable instrument, and thus exposures of the thorium-argon arc lamp for wavelength calibration were taken only a few times per night. During each run, spectra of rapidly rotating B type stars were observed to identify telluric absorption lines. Low metallicity stars with a range of effective

temperature were observed to correct for the blaze function of the spectrograph.

4. Data Reduction

The usual CCD image reduction procedures of overscan fitting, overscan subtraction, and zero subtraction were done using routines we developed in Interactive Data Language (IDL)[3]. Mapping and subtraction of scattered light in 2 dimensions, flat fielding in 2 dimensions, extraction of spectra from 2 dimensions to 1 dimension, wavelength calibration, blaze correction, and normalizing the continuum to unity were performed with tasks in the IMRED.ECHELLE package of the Image Reduction and Analysis Facility (IRAF)[4] following the general outline in the data reduction section of the HIRES users manual (Vogt 1994). Individual spectra were combined using our own IDL routine, SCOMBINE, which is based on IRAF's SCOMBINE task, which uses medians to robustly reject pixels influenced by cosmic-rays.

Figure 2 illustrates typical spectra of two Sgr dSph stars, one metal–rich and one metal–poor. Note that in the top spectrum, the Na I line at λ 6154 and the Ca I line at λ 6256 are non-detections, and the Na I line at λ 6161 has an equivalent width of 14 mÅ, which is roughly twice our detection limit of ~ 7 mÅ.

Heliocentric radial velocities, $v_{\rm helio}$, were computed from the observed wavelengths of a set of 15 moderately strong absorption lines. The velocities are listed in the last column of Table 2. The average $\rm v_{helio} = 143.5$ km/s with a standard deviation of 7.7 km/s. All stars were within 2 standard deviations from the average. Therefore, these stars are all bona fide radial velocity members of the Sgr dSph galaxy.

Identification and measurement of the equivalent width (EW) of atomic lines was accomplished by use of the semi-automated routine GETJOB (McWilliam et al. 1995a). Table 3 shows the measured EWs in mÅ. Values listed as "..." in Table 3 either represent lines that: (1) fell in gaps of wavelength coverage, (2) were irrevocably corrupted by telluric absorption lines, night sky emission lines, cosmic rays, or bad columns on the CCD, (3) were not detected, or (4) were too strong to yield an accurate abundance. Entries marked with ":" are uncertain. Equivalent widths from GETJOB are not completely independent of the user; differences usually arise from decisions regarding continuum regions to be used, and over-riding the automated line fits. All abundances in this paper are based on EW measurements from TSH. We investigated the EW uncertainties by comparison with three stars measured by AMcW; also using GETJOB. We found typical 1σ random errors of 3–3.5 mÅ, with systematic uncertainties of the same magnitude.

---

[3]IDL is commercial software sold by Research Systems, Inc.

[4]IRAF is distributed by the National Optical Astronomy Observatories, which is operated by the Association of Universities for Research in Astronomy, Inc., under cooperative agreement with the National Science Foundation.

5. Chemical Abundance Analysis

Abundance analysis was performed using the spectrum synthesis program MOOG (Sneden 1973) and the Kurucz (1993) 64–layer model atmospheres. Abundances for almost all lines were derived by matching the observed line EWs from Table 3 with synthesis predictions. For the Y II line at 5402.8Å spectrum synthesis profile matching was used to determine the abundance for all stars, except 1-41 (where the line was not detected). The profile of a clean Ti II line, at 5418.8Å, was matched to estimate the instrumental broadening for the Y II line.

Line wavelengths, gf values and excitation potentials were taken from McWilliam & Rich (1994, MR94), supplemented with extra lines for the current work; the line list is presented in Table 4. Our abundance analysis was restricted to lines with EW $\leq$150 mÅ, because lines much stronger than this which are on the flat portion of the curve of growth are quite insensitive to abundance.

For Y, La, and Eu we included the hyperfine components in our abundance calculations. For many of our stars the barium lines were so saturated that it was not possible to compute reliable abundances. The La II lines, in particular, were very strong and the inclusion of hyperfine effects was crucial for reliable abundance analysis. The La hyperfine splitting, hfs, constants were taken from Lawler et al. (2001a). For Y II lines the hfs A constants of Wännström et al. (1994) were utilized. We note that the abundance effects of hfs for Y II lines was very small, usually within 0.01 to 0.03 dex of the single line result. For Eu we employed the hfs line list of McWilliam et al. (1995b), which was computed using the constants of Krebs & Winkler (1960), Arnesen et al. (1981) and Sen & Childs (1987); these studies clearly resolved individual hfs components so it is unlikely that there are any significant differences with the recent Eu hfs constants measured by Lawler et al. (2001b).

Through a series of spectrum synthesis experiments, using the Kurucz (1993) line list, we identified the least blended Y II lines in our spectra. We found that Y II lines at 5546.0, 6613.7, 6858.2 and 7450.3 Å were severely blended in our stars; Y II lines at 5509.9 and 7264.2Å were blended, and not used, but might provide realively reliable Y II abundances with spectrum synthesis profile matching.

For abundance ratios relative to the Sun we adopted the solar abundance scale of Grevesse & Sauval (1998), but with a solar iron abundance of ϵ(Fe) = 7.50[5].

Our initial effective temperature (T_{eff}) estimates were based on broad–band colors, dereddened with the assumed SL95 reddening value of E(V−I) = 0.18, the reddening relations of Winkler (1997), and the color-temperature calibrations of Alonso et al. (1999; hereafter A99). An error in the A99 calibration formula produced spurious temperatures for all but the (V−I) colors (see Alonso et al. [2001] for the correct formula); however, we were unaware of the error until late

[5] $\epsilon(M) = log_{10}N(M) - log_{10}N(H) + 12$, where $N(M)$ is the abundance of element M by number

in the present work. The large dispersion in computed photometric temperatures led to some confusion and we were skeptical about their reliability, although the (V−I) results appeared the most reasonable. In order to check the photometric temperatures we computed excitation $T_{\rm eff}$ values from the abundances of our 75 Fe I lines.

The excitation temperatures and microturbulent velocities were computed using a program AUTO_AB, written by A.McW. The program uses MOOG and the Kurucz (1993) 64–layer model atmosphere grid to iteratively compute the Fe I abundances with different model atmosphere temperatures. When the Fe I abundances are independent of line excitation potential the correct temperature model has been found. This procedure requires that the microturbulent velocity parameter is known, which is reached when the abundances of the Fe I lines are independent of line EW. Thus program AUTO_AB consists of two loops: the inner loop iterates on the microturbulent velocity parameter, and the outer loop iterates on the model effective temperature. Inputs to the program are the gravity, metallicity, EWs and the starting values for temperature and microturbulent velocity. If spectroscopic gravities are also required a further iterative loop is performed to bring the abundances of ionized and neutral species into concordance. We caution, however, that when both spectroscopic temperatures and gravities are derived together the positive covariance between these parameters can result in a solution unexpectedly far from the true values. In this work, our excitation temperatures were computed using the photometric gravities.

The adopted temperatures are particularly important for our relatively cool K–giant atmospheres; near $T_{\rm eff} \sim$ 4000 °K, Ca, Ti, and Fe go from mostly neutral to mostly ionized in the line–forming region, and as a result the computed abundance ratios can become particularly sensitive to the assumed $T_{\rm eff}$. The derived excitation temperatures rest heavily on the small number of very low excitation Fe I lines, which we know are formed in the upper–most layers of the atmospheres, where the models are least reliable. Furthermore, recent investigations into the effects of granulation (e.g Steffen & Holweger 2002), show large differences from the classical one–dimensional LTE abundances for low excitation lines in the Sun. Although such effects have yet to be studied for red giant atmospheres it seems likely that similar abundance corrections for low excitation lines might exist, which would alter the derived excitation temperatures. The sense of the granulation corrections for the Sun indicates that excitation temperatures would be over-estimated. However, it should be noted than Ivans et al. (2001) found no significant difference between their spectroscopic and color temperatures for red giant stars in the globular cluster M5, which has [Fe/H] = −1.2.

Given the above uncertainties, we decided to employ the iron ionization equilibrium (i.e. ϵ(Fe I)=ϵ(Fe II)) to provide an additional spectroscopic temperature indicator, $T_{\rm ion}$. Given an assumed gravity the ionization temperature, $T_{\rm ion}$, is the temperature which forces the abundance of Fe I and Fe II lines to agree. We computed gravities using the published photometry and the following equation:

$$\log g = \log({\rm M}/{\rm M}_{\odot}) - \log(L/L_{\odot}) + 4\,\log({\rm T}_{\rm eff}/{\rm T}_{\rm eff,\odot})\,. \qquad (1)$$

Since the photometric gravity requires an input temperature an iterative method was used to determine a self-consistent T_{eff} value for each star: Initial values for T_{eff} and $\log g$ were adopted and an abundance analysis performed, which provided estimates of [Fe/H] and [α/Fe]. These four atmosphere parameters were then used to estimate the bolometric correction, B.C., by interpolation of the tables computed by Kurucz (1993). The observed V magnitudes, reddening, and distance modulus of SL95 permitted a calculation of the bolometric luminosity, M_{bol}. Padova isochrones (Girardi et al. 2000) were then employed to calculate the age of the star and the stellar mass consistent with the assumed temperature, luminosity and metallicity (see §6). With the derived stellar mass, Eqn. 1 was used to recompute the gravity. Next an abundance analysis of Fe I and Fe II lines was performed with the gravity fixed (iterations on the microturbulent velocity parameter were necessary); the temperature of the model atmosphere was then altered until ionization equilibrium was achieved (i.e. ϵ(Fe I)=ϵ(Fe II)). The new values of T_{eff}=Tion, $\log g$, [Fe/H], and [α/Fe] were used as inputs into the next loop of the iterative calculations. Convergence was assumed when the change in $\log g$ fell below 0.10 dex.

We note that use of ionization equilibrium inherently assumes that non–LTE over ionization effects are insignificant. If non–LTE over ionization of iron is important in these stars then our derived temperatures over-estimate the true values. Calculations by Thévenin & Idiart (1999) suggest that non–LTE over ionization of Fe I is significant in metal–poor stars, with the abundance correction reaching 0.3 dex at [Fe/H] = −2.5, while at [Fe/H] = −0.5 their correction is ∼0.05 dex. Non-LTE calculations by Steenbock (1985) for the red giant Pollux suggested corrections for Fe I lines of order ∼0.05 dex. The non–LTE over ionization should be relatively small for cool, metal–normal, stars as the temperature provides very few UV photons, and line blanketing in the blue ensures that those photons have a short path length. Empirical evidence suggestive of non–LTE over ionization of Fe I has been found in metal–poor stars (e.g. Ivans et al. 2001, Fulbright 2000). However, given that most of our sample of Sgr stars are very cool and more metal rich than [Fe/H] ~ -0.5 the non–LTE corrections are unlikely to exceed 0.05 dex, which would lead to an overestimate of ~ 50 °K for our ionization equilibrium temperatures.

In Table 5 we compare temperatures derived from iron excitation, iron ionization and photometric methods for our sample of Sgr stars. The mean difference $(T_{ex} - T_{ion}) = 33$ °K, with a 1σ about the mean of 92 °K. The 33 °K mean difference is consistent with a net zero difference between the two spectroscopic methods at the 1.3σ level. If both spectroscopic methods contribute equally to the 92K dispersion, then the 1σ uncertainty of an individual measurement is 65 °K. However, the mean 1σ excitation temperature uncertainty is 80 °K, computed from the scatter in Fe I abundances; this suggests that ionization temperatures have a 1σ uncertainty near 45 °K.

We find an unexpectedly large mean difference between temperatures based on ionization equilibrium and those based on photometry: $(T_{ion} - T_{phot}) = 249$ °K, with a 1σ of 112 °K. The excitation temperatures are on average 282 °K hotter than the photometric values, with a 1σ of 100 °K. The temperature difference between photometric and spectroscopic methods could be due to an under estimate of the reddening by SL95. However, to resolve the two temperature scales, a

reddening of E(B−V)$\sim$ 0.32 would be required, which is 0.19 mag higher than the SL95 estimate and completely inconsistent with their estimated 0.02 mag uncertainty in E(B–V).

In order to check for systematic errors in the temperature scales we decided to derive spectroscopic and photometric temperatures for the nearby K2III red giant star, Arcturus. Arcturus is a useful standard star as its temperature, metallicity, and gravity are very similar to many of our Sgr stars. Furthermore, the atmosphere parameters for Arcturus can be constrained very well thanks to its close proximity: the Hipparcos parallax implies a distance of 11.25 ± 0.09 pc, so the reddening is insignificant. Also, the large angular diameter, over 20 milli-arc seconds, permits an accurate estimate of the effective temperature.

The median of 6 literature estimates (Blackwell et al 1975, Augason et al. 1980, Blackwell et al. 1986, Bell & Gustafsson 1989, Blackwell et al. 1990, Alonso et al. 1999) for the total flux from Arcturus was found to be 4.95×10^{-12} W/cm^2; with this value and the limb–darkened angular diameter of Perrin (1998) we computed an effective temperature of 4290 °K, with an uncertainty of ±10 °K. We note that Alonso et al. (1999) adopted a lower total flux for Arcturus than any other study, at 4.83×10^{-12} W/cm^2, which indicates an effective temperature of 4268 ± 55 °K.

Alonso et al. (1999) adopted a temperature for Arcturus of 4233 ± 55 °K, based on the infrared flux method, which is consistent with our result. However, the average Arcturus effective temperature computed from the Alonso et al. (1999, 2001) color-temperature calibrations and literature (B−V) and (V−K) colors in the *SIMBAD* database is 4300 °K (17 °K *rms* scatter), and agrees well with T_{eff}=4280 °K from McWilliam (1990) based on 10 broad–band colors. The adopted T_{eff}, with extant photometry and the *Revised Yale Isochrones* (Green et al. 1987) indicate that Arcturus has a mass of $\sim 1.1 \pm 0.1 M_\odot$, and a gravity of $\log g = 1.64$ dex with an uncertainty of order ±0.05.

For our spectroscopic analysis of Arcturus the EWs were measured from the high quality spectrum of Hinkle et al. (2000), characterized by R=150,000 and S/N=1000 per pixel. Our initial analysis indicated an excitation temperature for Arcturus of 4400 °K with 1σ of 40 °K. However, upon inspecting the plot of abundance versus excitation potential, we noticed a clump of 8 high–excitation lines well above the main group of abundance values, and we suspected that these lines may be affected by blends. The lines are at the following wavelengths: 6173.34, 6380.75, 6481.88, 6820.37, 7007.98, 7090.39, 7130.93, and 7142.52 Å. When we eliminated these lines from the analysis the excitation temperature for Arcturus was reduced to 4330 ± 34 °K, entirely consistent with our value for the photometric effective temperature. The ionization temperature derived for Arcturus was 4294 °K without the 8 suspect lines and 4280 °K using all lines.

Thus we conclude that the color temperature, excitation temperature, ionization temperature, and physical effective temperature of Arcturus are all consistent, with T_{eff}=4290 °K. The temperature based on ionization equilibrium of iron is more robust than the excitation temperature, probably because a few pathological lines can affect the slope of the abundance versus excitation potential regression more easily than they can change average abundances. However, it should be remembered that ionization temperatures are sensitive to the accuracy of the adopted gravity,

which in turn depends upon the reliability of the distance estimate.

When the 8 suspect lines were excluded from the spectroscopic analysis of the Sgr stars the average effect was to reduce the excitation temperatures by 54 °K, while the ionization temperatures changed by less than 5 °K; resulting in a mean difference ($T_{ex} - T_{ion}$) = −25 °K. Thus, agreement between the two spectroscopic temperatures actually improved slightly for the Sgr stars.

Given the self-consistency of the Arcturus temperature estimates and the agreement between ionization and excitation temperatures we decided to adopt a spectroscopic temperature scale for the Sgr stars. We prefer the ionization temperatures because of their insensitivity to small numbers of pathological lines. We must conclude that for some unknown reason the Sgr color–temperature relations are much redder than normal. This could occur because non-standard blanketing makes the stars appear too red, or because of an unusual reddening law in the direction of Sagittarius. In this regard it is interesting that the Galactic bulge red giants seem to be afflicted by a similar problem (e.g. Udalski 2003, Kubiak et al. 2002); since these two objects share a similar direction it may be that the answer lies with a non-standard reddening law.

The final adopted stellar parameters are shown in Table 6, which lists star name, bolometric correction (B.C.), bolometric luminosity ($M_{\rm bol}$) computed from the photometry, the adopted effective temperature ($T_{\rm eff}$), gravity ($\log g$), the total metallicity of the model [A/H], the microturbulence (ξ). The assumed typical 1–σ errors in the adopted stellar parameters are $\sigma_{M_{\rm bol}} = 0.15$ mag, $\sigma_{T_{\rm eff}} = 70$ °K, $\sigma_{\log g} = 0.15$ dex, and $\sigma_{\xi} = 0.05$ km/s. Table 6 lists the derived metallicities, [Fe/H], and abundance ratios, [X/Fe]. Note that here we adopt the average of [Ca/Fe], [Si/Fe], and [Ti/Fe] for the [α/Fe] ratio, because the abundances of these elements are much better defined than O or Mg due to the availability of many more lines. As is typically the case, systematic errors rather than random errors are the dominant source of uncertainty in our abundances. Propagating the errors in the adopted stellar parameters yields typical 1–σ errors of $\sigma_{[\rm Fe/H]} = 0.07$ dex and $\sigma_{[\alpha/\rm Fe]} = 0.07$ dex. Typical errors for other element ratios are listed in the last row of Table 7 as well as average abundances and standard deviations for the metal–poor and metal-rich groups.

Errors arising from systematic trends in the EWs can be estimated from the duplicate line measurements made by the two authors of this paper: The AMcW EWs led to slightly different atmosphere parameters and abundances, over the TSH scale: The largest changes were for I-245 with a 100K lower $T_{\rm eff}$ and microturbulent velocity lower by 0.2 Km/s. The derived [Fe/H] values were all within 0.05 dex of the values derived from the TSH EWs, while abundance ratios changed by less than 0.05 dex.

6. Ages

Ages were derived for each star by comparing the star's bolometric luminosity and effective temperature listed in Table 6 with isochrones interpolated for the star's derived metallicity using the Padova models (Girardi et al. 2000). We chose to do the interpolation of the age in the $M_{\rm bol} - T_{\rm eff}$

plane in order to avoid additional uncertainties introduced by adopting a specific color–temperature transformation. Padova models from Girardi et al. (2000) were used to generate isochrones at given metallicities; these were kindly provided to us by our collaborator Andrew Cole. The Padova models were calculated assuming a scaled-solar mix of elements. Because some Sgr red giants show significant departures from solar element ratios (primarily the three metal–poor stars), as we show below, we must take this into account when deriving their ages. The α elements and Fe are the main sources of opacity. Salaris, Chieffi & Straniero (1993) show that an isochrone for a model of a given [Fe/H] and [α/Fe] is nearly identical to that of a scaled solar model with an effective metallicity equal to

$$[\mathrm{Fe/H}]_{\mathrm{eff}} = [\mathrm{Fe/H}] + \log(0.638 \times 10^{[\alpha/\mathrm{Fe}]} + 0.362). \tag{2}$$

Therefore, we interpolate the age of a star using a Padova model with the derived $[\mathrm{Fe/H}]_{\mathrm{eff}}$. Effective metallicities are listed in Table 6. The derived ages (t) and age errors (σ_t) are listed in Table 5.

Errors in the derived age of each star were calculated by propagating the 1–σ errors in M_{bol}, $\mathrm{T_{eff}}$ and $[\mathrm{Fe/H}]_{\mathrm{eff}}$ assuming all three variables were uncorrelated. This should be an innocuous assumption, whose effect might be to somewhat inflate the calculated error relative to the true error. The age error is assumed to be

$$\begin{aligned} \sigma_{\mathrm{t}}^2 \;=\; & \left(\frac{\delta t}{\delta [\mathrm{Fe/H}]} \Big|_{[\mathrm{Fe/H}]_1}^{[\mathrm{Fe/H}]_2} \right)^2_{\mathrm{M_{bol},T_{eff}}} \times \sigma^2_{[\mathrm{Fe/H}]} \;+ \\ & \left(\frac{\delta \mathrm{t}}{\delta \mathrm{M_{bol}}} \Big|_{\mathrm{M_{bol,1}}}^{\mathrm{M_{bol,2}}} \right)^2_{\mathrm{T_{eff},[Fe/H]}} \times \sigma^2_{\mathrm{M_{bol}}} \;+\; \left(\frac{\delta \mathrm{t}}{\delta \mathrm{T_{eff}}} \Big|_{\mathrm{T_{eff,1}}}^{\mathrm{T_{eff,2}}} \right)^2_{\mathrm{[Fe/H],M_{bol}}} \times \sigma^2_{\mathrm{T_{eff}}} \end{aligned} \tag{3}$$

where we evaluated the partial derivative with respect to variable x from $x_1 = x - \sigma_x$ to $x_2 = x + \sigma_x$ while holding the other two variables fixed. Note that these errors do not take into account uncertainties in the theoretical models themselves. In short, there are serious limitations in our current understanding and parameterization of the relevant physics in red giant stars (opacities, convection theory, etc.) that could produce errors in the derived shape of theoretical giant branches, and thus produce additional systematic errors in our derived ages. For two recent reviews of the status of theoretical modeling of red giant stars, we refer readers to D'Antona (2001) and Salaris, Cassisi & Weiss (2002).

7. Results and Discussion

Below we discuss the distribution of metallicities, element ratios and ages in Sgr dSph stars, and how these constrain the amount of enrichment from type Ia SNe, type II SNe, and long–lived,

low–mass AGB stars, and the initial mass function. We conclude that the Sgr dSph formed stars and chemically enriched itself over a timescale of many Gyr; its star–formation rate was either slow or episodic, and outflow of chemically–enriched gas was important to its evolution. We also discuss how the complex evolution of the Sgr dSph gives us interesting insight into the hierarchical merging history of our Galaxy.

7.1. [Fe/H] and Age Distribution

In Figure 3, we show the dereddened CMD for the Sgr dSph stars with stars in the spectroscopic sample shown with color–coded symbols that reflect their derived effective metallicities. Note that the large spread in color for stars in the narrow metallicity range of $-0.39 \leq$ [Fe/H] ≤ -0.31 suggests a significant range in age for the stars. The populous red giant branch sequence at the reddest side of the CMD, which is very narrow in color, contains stars with a mix of metallicities, $-0.30 \leq$ [Fe/H] ≤ 0. Again, this suggests a range in ages because of the degeneracy of age and metallicity (red giants become redder if they are more metal–rich, but bluer if they are younger). It can be seen from Figure 3 that our selection of objects was slightly biased towards the old/metal-rich Sgr stars.

Figure 4 shows the age–[Fe/H] relationship for our Sgr dSph stars. The metallicities range from $-1.6 \leq$ [Fe/H] ≤ 0.0. The stars in our sample are all radial velocity members; furthermore, the unusual chemical compositions (as discussed below) indicates that they are not Galactic halo, bulge, or disk interlopers. Our high-dispersion abundances confirm the existence of a solar metallicity component as suggested by the strengths of the Ca II near-infrared triplet lines in low–dispersion spectra obtained by Ibata and collaborators (1996, private communication to TSH).

The metallicity spread in the Sgr dSph was inferred to be large, $-2.0 \lesssim$ [Fe/H] $\lesssim -0.7$, based on the wide distribution in colors of its red giant stars (Bellazzini et al. 1999). Bellazzini et al. performed a VI–band photometric survey over a wide area in 3 different Sgr fields. For ~ 100 stars on the upper red giant branch, they derived metallicities by interpolating fiducial sequences of Galactic globular clusters. This provided the best way of separating Sgr stars from Galactic foreground dwarfs and the estimating the metallicity distribution from photometry alone. They concluded that 80–90% of Sgr stars were metal–poor, [Fe/H] < -1. However our spectroscopic metallicities for most Sgr stars are significantly higher than this. This discrepancy is understandable because of the degeneracy of age and metallicity in color–magnitude diagrams. The derived ages of our stars vary from ~ 1.0 to 15 Gyr, hence many Sgr stars are significantly younger than globular clusters. Significantly decreasing the age of these stars would have yielded a much higher metallicity in the Bellazzini et al. analysis, reaching solar, as we find from our spectroscopy.

The age sensitivity of the red giant branch is small for ages $\gtrsim 3$ Gyr, and thus our derived ages for the stars older than this have large uncertainties. To compliment the field star data, we also show in Figure 4 data from 4 globular clusters that are members of the Sgr dSph (M54, Ter8,

Arp2, Ter7). Cluster ages, derived from the V magnitude of the cluster subgiant branch, were taken from Layden & Sarajedini (2000) and placed on the age scale of the Bertelli et al. (1994) isochrones. The Bertelli et al. models were the precursors of the Padova models that we use to derive the ages of our Sgr field stars, and their absolute age scales are roughly similar. In order to compare with our field star metallicities derived from high-dispersion spectra, we adopt [Fe/H] $= -1.55$ for M54 as derived by Brown, Wallerstein & Gonzalez (1999) from high-dispersion spectra of five M54 red giants; although a recalibration of the Zinn & West (1984) scale by Kraft & Ivans (2003) suggests that [Fe/H]$=-1.41$. For the other clusters without high-dispersion spectroscopy, we use metallicities from the catalog of Rutledge et al. (1997) that are derived from the strengths of the Ca II infrared triplet lines in low-dispersion spectra of red giants, but calibrated to the Carretta & Gratton [Fe/H] scale, which is based on high-dispersion spectroscopic abundances.

The spread in [Fe/H] and age of Sgr dSph stars indicates that star formation and chemical enrichment was prolonged, with a possible gap between metal–rich and metal–poor populations. It would be interesting to obtain high-dispersion spectra of stars in Ter 7, the cluster inferred to be ~ 4 Gyr younger than the other globular clusters, as well as additional intermediate-aged and older field stars in the Sgr dSph to flesh out the age-metallicity relationship. In Figure 4, the solid line shows the prediction from a simple chemical evolution model that assumes instantaneous recycling, a closed box, star formation that has gone to completion at the present time (i.e., the mass of gas at 15 Gyr is zero) and a star formation rate that is constant in time. Layden & Sarajedini (2000) suggested such a model was a good fit to the age-[Fe/H] relationship they derived from color–magnitude diagram analysis. (Note that they derived [Fe/H] from photometric methods rather than spectroscopy.) A model with a yield of $p = 0.0033 = 0.17\,\mathrm{Z}_\odot$ is implied by our data although this model does not fit the data very well. Note that this yield is much lower than the yield inferred from stellar nucleosynthesis. For comparison, the yield in the Galactic bulge, which is reasonably well fit by a simple closed box model, is $p = 0.7\,\mathrm{Z}_\odot$ (Rich 1990) and that implied by the the metallicity distribution function of the Galactic disk indicates the yield is $p = 0.50\,\mathrm{Z}_\odot$ (Pagel & Patchett 1975). Such a low yield in Sgr implies that the closed box assumption is probably not valid. In a simple outflow model, where the outflow rate is assumed to be proportional to the star formation rate ($\dot{M}_{gas} = \nu\psi$, where ψ is the star–formation rate and ν is the dimensionless proportionality constant), the age-metallicity relationship is identical to that predicted by the closed box model but with the effective yield being $p_{\rm eff} = p/\nu$. **Therefore, our Sgr results would imply $\nu \approx 0.28$ if the true yield is the same as that in the Galaxy, and thus mass loss has been a significant factor in the evolution of the Sgr dSph.**

7.2. Alpha Elements

In this paper, we discuss the element ratio [α/Fe] where α is taken to be the average of the Si, Ca, and Ti abundances; O and Mg abundances were not used in the present paper because of the uncertainty associated with their paucity of lines.

In the following plots of element ratios, our data on Sgr dSph stars will be shown as filled circles. For comparison, we plot as open circles the abundances for 2 field stars in the Sgr dSph derived from high-dispersion spectroscopy by Bonifacio et al. (2000). In addition, we plot as an open star symbol the average abundance of 4 stars in the globular cluster M54, which is member of the Sgr dSph, obtained from high-dispersion spectra by Brown, Wallerstein & Gonzalez (1999). We discuss these studies in detail in §7.5.

Figure 5 shows that the most metal–poor Sgr dSph stars exhibit an enhanced [α/Fe] ratio, similar to Galactic halo stars, which have an average [α/Fe] = +0.35 (McWilliam 1997); however, for stars with [Fe/H]> -1, it is clear that the α elements are deficient by $\sim$0.1 dex relative to the solar neighborhood trend. The metal-rich Sgr stars also appear to have a fixed [α/Fe] ratio. The standard interpretation of such an observation (e.g. Wheeler et al. 1989, McWilliam 1997) is that the ratio of type Ia/type II SNe ejecta incorporated into the metal-rich Sgr stars is larger than in solar neighborhood stars of similar metallicity. This could be due to episodic star–formation, meaning that the star–formation rate went to zero for an appreciable length of time between the formation of the metal–poor and metal–rich stars, allowing type Ia SNe to continue to explode and enrich the interstellar medium in Fe when no accompanying type II SNe produced additional α elements. Alternatively, if the star–formation rate was continuous with time then it must have had a shorter e-folding timescale than that of the solar neighborhood. For reference, Scalo (1986) finds that the average star–formation rate, $\psi(t)$, in the solar neighborhood was 2 to 3 times its current star–formation rate, $\psi(T)$. If we assume a simple star–formation rate of the form $\psi \propto e^{-t/\tau}$ for the Galactic disk in the solar neighborhood, then $\tau = 0.62T \sim 7$ Gyr if the current age of the disk is 12 Gyr. Deficiencies in the α elements have long been predicted for low-mass galaxies (e.g. Matteucci & Brocato 1990, Gilmore & Wyse 1991). A similar result was found for disk stars with large Galactocentric radii in the study by Edvardsson et al. (1993), where it was concluded that star formation proceeded at a slower pace in the outer disk than in the inner disk.

An interesting feature of Figure 5 is the apparent constant value of the [α/Fe] ratios above [Fe/H]~ -0.6 dex. If this is correct, then the ratio of type Ia to type II SNe must have been roughly constant over this metallicity range.

How much type Ia ejecta does the observed [α/Fe] imply for the Sgr stellar populations? The theoretical yields of type II SNe are fairly uncertain because the mass cut and explosion energy are imposed parameters rather than derived from the models themselves (e.g., Woosley & Weaver 1995; hereafter WW95). Therefore, to estimate the relative amount of type Ia verses type II SNe enrichment, we assume the average yield of type II SNe integrated over the initial mass function (IMF) is equal to the average observed for Galactic halo stars, $[\alpha/\mathrm{Fe}]_{\mathrm{II}} = +0.35$ (McWilliam 1997). Models of type Ia SNe are uncertain because we do not yet know the exact progenitors. Are these double CO white dwarfs whose merger is induced by gravitational wave radiation, or a CO white dwarf accreting material from a Roche-lobe filling red giant companion? However the inherent mechanism is believed to the explosion of a CO white dwarf because it produces enough radioactive Ni and Co to power the observed light curve. We adopt the theoretical yields of the

popular W7 model of type Ia SNe from Thielemann, Nomoto & Yokoi (1986, hereafter TNY86), but we note that the yields are uncertain particularly for the intermediate-mass elements which are not constrained well by direct observations. We note that in both the type Ia and type II SNe models, the predictions for Ti are not well correlated with Si and Ca, despite the fact that Ti correlates well with them in Galactic and Sgr dSph stars. Therefore, we will adopt the averages of the Si and Ca ratios for the theoretical [α/Fe] yields of SNe; for the W7 model, $[\alpha/\mathrm{Fe}]_{\mathrm{Ia}} = -0.36$.

It is difficult, if not impossible, to place reliable uncertainties on the theoretical yields for type Ia SN, because the errors are dominated by unknown systematic effects; neither TNY86, nor Thielemann et al. (1984) quantify the uncertainties, although comparison with the solar abundance distribution is made at the level of 0.3 dex.

The 7 type Ia SN models investigated by Iwamoto et al. (1999) show a dispersion in the predicted Si/Fe yield ratio of 0.16 dex, which are particularly sensitive to the deflagration to detonation transition; the highest Si/Fe yeilds, near -0.8 dex, occurs when the density ahead of the flame is artificially decreased from 2.2 to $1.7 \times 10^7 gcm^{-3}$.

For a stellar population with a given α-element ratio, [α/Fe], the fraction, f, of Fe that came from type Ia SNe in that population is given by Equation 4; note that this assumes zero contribution of α elements by other sources, such as novae.

$$f = \frac{\left(10^{[\alpha/\mathrm{Fe}]} - 10^{[\alpha/\mathrm{Fe}]_{\mathrm{II}}}\right)}{\left(10^{[\alpha/\mathrm{Fe}]_{\mathrm{Ia}}} - 10^{[\alpha/\mathrm{Fe}]_{\mathrm{II}}}\right)} \,. \tag{4}$$

For the metal-poor Sgr stars $[\alpha/\mathrm{Fe}] = +0.27$, from which we infer $f = 0.21$ if the IMF in the Sgr dSph was the same as that in the Galactic halo. Note that [α/Fe] declines with metallicity even among the metal-poor group; although this is not highly significant given the errors and the numbers of stars observed, it suggests that the metal-poor population could be enriched by type Ia ejecta. In regard to the question of whether or not the IMFs in dSphs and the Galaxy are similar, we note that the low-mass end of the IMF in the Ursa Minor dSph has been shown to be indistinguishable from low-metallicity Galactic globular clusters over the mass range of 0.3 – 0.85 $M_\odot$ (Wyse, et al. 2002). In addition, the bulk of the present evidence suggests that little variation occurs in the IMF at different metallicities or in different environments; see the recent review by Kroupa (2002).

The median α-element ratio in the metal-rich Sgr population, at $[\alpha/\mathrm{Fe}] = 0.0$, implies a fraction, $f = 0.68$, of iron from type Ia SNe; under the assumption that the Sgr dSph IMF was the same as in the Galactic halo. The standard deviation in the [α/Fe] ratio of 0.05 dex, implies that the acceptable range on the fraction is $0.62 \leq f \leq 0.75$. For comparison, the α-element ratio of solar neighborhood stars, with metallicities equal to the mean metallicity of the metal-rich Sgr stars, is $[\alpha/\mathrm{Fe}] = +0.10$, for which $f = 0.54$.

The lowest metallicity star in the Sgr dSph has $[\alpha/\mathrm{Fe}] = +0.32 \pm 0.07$, which is similar to

those of Galactic halo stars. What constraints can this place on the upper-mass end of the IMF in the Sgr dSph? Unfortunately, no definitive answer can be made because of the uncertainties in the type II SNe models (e.g., Gibson 1998, WW95), but a comparison is certainly worthwhile.

WW95 published type II SNe yields for a range of initial stellar metallicities, and their low metallicity models are relevant for comparing with this Sgr star, which has [Fe/H] = −1.6. We have calculated the yields weighted over a given IMF, where

$$\Phi(m) \propto m^{-(1+x)} \tag{5}$$

is the number of stars formed with initial mass in the range m to $m + dm$, and the slope of the IMF is x. Note that $x = 1.35$ is the slope derived by Salpeter (1955), and $x = 2.3$ is the slope derived by Miller & Scalo (1979) for $m > 10$ $M_\odot$ in the solar neighborhood. We assume the initial mass range for type II progenitors is $10 \leq (m/M_\odot) \leq 50$. We use the ejected masses calculated for the WW95 models as tabulated by F. Timmes (2002, private communication to TSH) and the solar abundances of Grevesse & Sauval (1998). The WW95 models predict that Ti should behave more like an Fe-peak element than an α-element, contrary to what is observed in the Galaxy and the Sgr dSph. Therefore, we adopt the average of Si and Ca for [α/Fe].

The WW95 models with initial stellar metallicities $Z = 10^{-4} Z_\odot$ have [α/Fe] yields that are nearly constant as a function of stellar mass; $+0.36 \leq$ [α/Fe] ≤ 0.35 for $0 \leq x \leq 3$. This element ratio is encompassed by the 1–σ upper limit for the Sgr star, but we can place no constraint on the IMF slope. Note that altering the progenitor mass range will not change appreciably the predicted [α/Fe]. The $Z = 10^{-2}$ models are probably more relevant to our [Fe/H] = −1.5 Sgr star, because we expect many more stars of this metallicity contributed to its enrichment. The predicted yields of the $Z = 10^{-2}$ models are sensitive to the IMF slope, but the models imply a surprisingly low [α/Fe] yield; [α/Fe] = +0.32 for $x = -0.9$, and [α/Fe] = $+0.26, +0.11$, and 0 for $x = 0, 1.35$, and 2.3, respectively. A proper prediction of the element ratios would necessitate a full chemical evolution model, but that is not worthwhile given the uncertainties on the present yields and the poorly–constrained star–formation rate.

Thus, for the time being, all we can say about the upper-mass end of the IMF in the Sgr dSph is that it greatly resembled that of the Galactic halo. When the yields of Type II SNe are on firmer footing, we may be able to place firmer constraints on the upper-mass end of the IMF, which is a crucial piece of information to determine because this sets the amount of energy available to power galactic winds.

An issue of interest is whether there is a trend of [α/Fe] with [Fe/H] for the metal-rich Sgr stars. Figure 5 shows a hint of a downward trend, but the slope isn't significantly different from zero. A zero slope would imply a constant ratio of type II to type Ia SNe that might arise from a steady star-formation rate, whereas declining [α/Fe] ratios are expected in the aftermath of a star formation burst.

7.3. Aluminum and Sodium

In Figure 6 we show comparisons of [Al/Fe] and [Na/Fe] in the Sgr dSph with the results for solar neighborhood stars from Chen et al. (2000). The Sgr stars with [Fe/H] < -1 possess Galactic halo–like abundances of Al and Na, as we see for the α elements. In the Fulbright (2000, 2002) sample of metal-poor stars in the solar neighborhood, the averages for halo stars with Galactic rest frame velocities $v_{\rm GRF} < 300$ km/s and $-2 <$ [Fe/H] < -1 are [Na/Fe] $= -0.09$ and [Al/Fe] $= +0.23$, similar to the metal-poor Sgr stars. Note that Fulbright finds a population of halo stars with unusual chemical abundance ratios in his sample, but these exclusively have $v_{\rm GRF} > 300$ km/s, and hence we omit them from the calculation of the halo average. The halo stars with unusual chemical abundances are on orbits that take them far into the Galactic halo (maximum Galactocentric radii $\gtrsim 20$ kpc). The relevance of these stars to the question of whether dSph–like fragments merged to form the Milky Way halo will be discussed in §7.7.

One metal-poor Sgr star stands out with Na and Al ratios very different from the Galactic halo. This is star 1−73 with [Fe/H] $= -1.09$ which shows a large enhancement of Al, [Al/Fe] $= +1.1$ dex (so large that it is not plotted in Figure 6), a small enhancement in Na, [Na/Fe] $= +0.2$, and a large deficit of O, the upper-limit being [O/Fe] $\lesssim -0.8$ dex. This appears to be the same phenomenon seen in some Galactic globular cluster red giants, which are probably due to self-polllution with proton-burning products in the stellar atmosphere, with depleted O and enhanced Na and Al (e.g. Kraft et al. 1997); although primordial abundance variations may play a role (e.g. Ivans et al. 1999, Sneden et al. 1997). At [Fe/H]$=-1.09$ the metallicity of 1−73 is significantly different from the mean metallicity of M54 stars, [Fe/H] $= -1.55$ (Brown, Wallerstein & Gonzalez 1999). Thus we believe this star is a field star and not a cluster member, although its position on the sky and radial velocity are similar to M54 stars.

Unfortunately, with only one Al-rich object we cannot estimate a lower limit to the frequency among Sgr field giants; in this study we find 7%±7%. In the Galaxy, envelope proton burning appears to be a phenomenon limited to some (but not all) Galactic globular cluster stars. Among the field red giants in the Galactic halo Fulbright (2000, 2002) found no stars with evidence of envelope nucleosynthesis of Al, from 168 stars investigated. Clearly, if future studies establish that ∼7% of Sgr giants possess enhanced Al, produced by proton burning, then very few Sgr–like dwarfs could have been incorporated into the Galactic halo field. Additional searches for Sgr field stars with similar signs of proton-burning would be very interesting.

For the stars with [Fe/H] > -1 in the Sgr dSph, both Al and Na are deficient relative to the solar neighborhood trend by ~ 0.4 dex. Although such low [Na/Fe] and [Al/Fe] ratios are very rare, they are not unheard-of in the Galaxy: Nissen & Schuster (1997) found four halo field stars ([Fe/H] ~ -1.0) with low [α/Fe] $\sim +0.05$, and [Na/Fe] ~ -0.3 dex. Brown et al. (1997) found that the young globular clusters Rup 106 and Pal 12 ([Fe/H]$=-1.45$ and -1.0, respectively) possess near-solar [α/Fe] with [Na/Fe] $= -0.50$ and -0.26 dex respectively; for aluminum there was an upper limit only for Pal 12, at [Al/Fe] ≤ -0.37. King (1997) found a common proper-motion pair

in the halo ([Fe/H] = −1.50) with solar [α/Fe] and [Na/Fe]=−0.4 dex. Fulbright (2000, 2002) finds $\sim$ 25% of his sample has $-0.3 \lesssim$ [Na/Fe] $\lesssim -0.7$ and $-2.6 \lesssim$ [Fe/H] $\lesssim -1.4$, and these are the outer halo stars with unusual chemical abundances as noted above. Notable among Fulbright's stars is BD+80 245 (originally identified as having low [α/Fe] by Carney et al. 1997), with [α/Fe]=−0.13 and [Na/Fe]=−0.50 dex.

The metal-rich Sgr stars are similar to the Al and Na deficient Galactic halo stars in that they also exhibit low [α/Fe] ratios; however, we are unaware of *any* Galactic stars with [Na/Fe]$\sim$−0.4 dex at metallicities as high as the metal-rich Sgr stars, $-0.6 \lesssim$ [Fe/H] $\lesssim 0$.

The majority of sodium and aluminum synthesis occurs during carbon and oxygen burning in massive stars, which ultimately end as type II SNe. (Na synthesis is also sensitive to the neutron excess, which makes the [Na/Fe] yield metallicity-dependent, e.g. Pardo et al. 1974). We conclude that the Al and Na deficiencies seen in Sgr dSph stars are due to a paucity of nucleosynthesis products from massive stars relative to type Ia ejecta. This is in qualitative, and quantitative, agreement with the observed deficiency in [α/Fe] ratios. The Al and Na deficiencies are larger than the α–element deficiences, which can be understood if type Ia SNe produce small amounts of α elements and very little Na or Al. This is exactly what the predictions are for type Ia; the yields from Thielemann, Nomoto & Yokoi (1986) are $[\mathrm{Na/Fe}]_{\mathrm{Ia}} = -4.00$ and $[\mathrm{Al/Fe}]_{\mathrm{Ia}} = -1.83$. Using Eqn. 1, with the yields for type II SNe again taken to be the averages of Fulbright's halo stars, $[\mathrm{Na/Fe}]_{\mathrm{II}} = -0.09$ and $[\mathrm{Al/Fe}]_{\mathrm{II}} = +0.23$, we derive the fraction of Fe created in type Ia SNe in the Sgr metal-rich stars. From [Na/Fe], we find $f = 0.49$ with the $\pm 1\sigma$ limits giving $0.29 \leq f \leq 0.63$. From [Al/Fe], we find $f = 0.73$ with $\pm 1\sigma$ limits giving $0.63 \leq f \leq 0.81$. Thus the fraction of iron from Type Ia SNe in the metal-rich Sgr population implies $f \approx 61\%$.

Note that we would get essentially the same values of f if we assumed that type Ia SNe make *no* significant amount of Na or Al, because the theoretical yields of [Na/Fe] and [Al/Fe] for Type Ia are so much smaller than that inferred for Type II SNe. If type Ia SNe make *any* Na or Al, or if the Galactic halo composition contains iron from some type Ia SNe (which seems likely considering that some 9 to 10 $M_\odot$ stars end as type Ia SNe) then the value of f must be increased further. If we assume Type Ia make no α elements then the fact that our metal-rich Sgr stars have an average of [α/Fe] = 0.0 implies $f = 0.50$ or 0.55 depending on whether one assumes the average for Galactic halo stars is [α/Fe] = 0.30 or 0.35 dex, respectively (see McWilliam 1997). For the [α/Fe] ratios to give a value of $f = 61\%$, as implied by the Na and Al ratios, then type Ia SNe must produce some α elements with a yield in the range of $[\alpha/\mathrm{Fe}]_{\mathrm{Ia}} = -0.44$ to -0.68 dex.

Therefore, we get a very consistent picture when we consider the observed Na, Al, Si, Ca and Ti abundances relative to Fe, from which we conclude that each of these element ratios can be explained if ≈ 60 to 70% of the Fe in the metal-rich Sgr population was synthesized by type Ia SNe and the remainder by type II SNe.

7.4. Neutron-Capture Elements

In Figure 7 we present the trend of [La/Fe] with [Fe/H]. While the metal–poor stars, with [Fe/H]=−1.1 to −1.6 appear quite similar to the Galactic halo in the figure, the more metal–rich stars show a steady increase in La enhancement with increasing [Fe/H], up to [La/Fe]$\sim$ +1.0 dex. The [La/Fe] trend suggests that there was a rough progression of metallicity with time, and that either the production of neutron-capture elements increased, or the efficiency of iron production decreased steadily. Iron from type Ia SNe might explain a reduced iron production rate, due to the decreasing probability that mass transfer to a white dwarf will exceed the Chandrasekhar limit for a population of older, and hence less massive, secondaries. In contrast, the trend of [Y/Fe] with [Fe/H], seen in Figure 8 is close to the solar ratio for all but the most metal-rich stars. We note that our Y abundances are significantly higher than the values found by Bonifacio et al. (2000).

Except in the most metal–poor stars ([Fe/H]$\leq$−2.5) La is thought to be produced mostly by the s–process; the solar s–process fraction for La is estimated at 75% (Burris et al. 2000). To investigate the neutron source for La in the Sgr dSph stars we show the [La/Eu] ratios in Figure 9; it is clear that [La/Eu] is increasingly dominated by the s–process at higher [Fe/H]. The average of the three highest [Fe/H] stars have super-solar [La/Eu]$\sim$ +0.15 dex; although this is dominated by one star. However, the Bonifacio et al (2000) [La/Eu] points support the value of the highest star, near +0.3 dex.

We note that because of the particularly small neutron-capture cross sections of the barium isotopes [Ba/Eu] is especially sensitive to the ratio of s to r–process elements; thus, we normally favor the use of [Ba/Eu] as a neutron-capture diagnostic. However, because the Ba lines in our spectra are very strong (150 to 400mÅ) they lie on the flat portion of the curve of growth, and are not very sensitive to abundance. For this reason [La/Eu] is probably a more reliable neutron-capture diagnostic in our sample of Sgr dSph stars than [Ba/Eu], despite the less favorable neutron-capture cross sections of La relative to Ba.

Since AGB stars are the dominant source of heavy s–process elements at Galactic disk metallicities (see Travaglio et al. 1999), the Sgr dSph heavy element abundance enhancements indicate a significant contribution from AGB nucleosynthesis, which increases relative to iron at higher [Fe/H].

Figure 10 shows a plot of [La/Eu] versus [La/H]: The horizontal dotted lines represent [La/Eu] for $s-$ and r-process composition; it is clear that at low [La/H] the Sgr stars were near the pure r-process value, similar to the Galactic Halo. The solid line shows the locus of [La/Eu] resulting from an addition of pure s-process material to the halo ratio with [La/H]=−0.8 dex, and the dashed line shows the locus arising from addition of pure s-process material starting with halo composition at [La/H]=−0.3 dex. Note that addition of pure s-process material gives the steepest possible slope; shallower slopes result with the addition of r-process material: the dot-dashed line shows the locus of halo composition plus 95% s-process and 5% r-process La. The available data are best fit with the addition of 97% s-process plus 3±3% r-process La composition, starting [La/H]=−0.3 dex; a point corresponding to the most metal-poor star in the metal-rich Sgr population, at [Fe/H]=−0.61

dex. This suggests that the halo-like [La/Eu] ratios, characteristic of a dominantly r-process origin, persisted in the Sgr gas up until [Fe/H]~-0.6 dex. More data are required to accurately determine the extent of the r-process contribution to the metal-rich Sgr stars, particularly for the more metal-poor Sgr stars.

Figure 10 indicates that the halo s/r mix of neutron-capture elements persisted until [Fe/H]$\simeq-0.6$ dex, despite the [La/Fe] enhancement of $\sim$0.3 to 0.4 dex at this metallicity (see Figure 7). This enhancement in [La/Fe] suggests that either the rate of iron production decreased, or the rate of production of predominantly r-process, halo-like, neutron-capture composition increased.

Our [Eu/Fe] abundance ratios, in Figure 11, demonstrate that it is dangerous to draw conclusions about the neutron-capture process responsible for europium by comparison with iron. Figure 11 shows [Eu/Fe] enhanced in metal-rich Sgr dSph stars, as compared to the trend seen in the solar neighborhood. Although the solar system Eu is 97% r-process it would be incorrect to assume that the observed enhancement is due to extra r-process material; as shown in Figure 10 the Eu abundances for the most metal-rich Sgr stars are consistent with a halo composition plus large s-process enhancement.

In Figure 12 we present a plot of [La/Y], showing that the heavy s–process element lanthanum is enhanced more than the light s–process element yttrium in the metal–rich Sgr dSph stars ([Fe/H]$geq-0.6$), with [La/Y] = $+0.45\pm0.02$ dex, roughly independent of metallicity. We note that the Bonifacio et al. (2000) results do not agree with the present work. In addition, two of the three metal-poor stars in the plot show evidence for slightly enhanced [La/Y] ratios; although this might be explained by noise enhancement of the apparent equivalent widths of the weak Y II lines.

The unusual [La/Y] ratios seen in the Sgr stars might be understood by either rapid, or slow, neutron capture nucleosynthesis.

With regard to rapid neutron capture, Wasserburg et al. (1996) showed that there exist at least two r-process sites in the Galaxy, with very different rates; the low-frequency and high-frequency events dominate the synthesis of r-process elements below and above A=130, respectively. Therefore, unusual heavy (e.g. Ba, La, Nd) relative to light (e.g. Sr, Y, Zr) neutron-capture element ratios, [hs/ls], may be obtained from abnormal mixtures of material from the two r-process sites: our observed high [hs/ls] ratios in the metal-rich Sgr stars would require relatively more production from the high-frequency r-process events. Although the site of the r-process has not yet been confirmed, if it is assumed to occur during type II SNe events, a niave interpretation would suggest that the SGr dSph contained more r-process material from low-mass type II SNe. SCS01 suggested that the unusual [Ba/Y] ratios in their sample of stars from three Local Group dSph galaxies were due to an unusual mix of high and low r-process events. We note that the SCS01 stars were much more metal-poor (at [Fe/H]$leq-1.4$) than our sample of Sgr stars with enhanced [La/Y].

Given the strong s-process signature, indicated by the [La/Eu] ratio, in the most metal-rich Sgr stars, it seems very unlikely that the high-frequency r-process sites of Wasserburg et al. (1996) could

be responsible for the observed high [La/Y] ratios. However, the enhanced [La/Y] ratio in the most metal-poor star of the metal-rich Sgr population, I-150, is not consistent with this picture, because it's halo-like [La/Eu] ratio suggests predominantly r-process material. The apparent contradiction my be solved by appealing to measurement errors, somewhat s-process enhanced [La/Y] for the metal-poor Sgr stars, or by an initial r-process enhanced [La/Y] ratio near [Fe/H]~-0.6 replaced by an s-process enhanced ratio at [Fe/H]~-0.1.

The s-process [hs/ls] ratios in AGB stars is predicted to depend on the metallicity of the s-process site (Busso, et al. 1999, Busso, et al. 2001). AGB s-process nucleosynthesis in low mass stars begins with protons ingested from the envelope into the helium inter-shell region, most likely during the "third-dredge-up" (TDU) after He shell flash. These protons are consumed in the $^{12}C(p,\gamma)^{13}C$ reaction, resulting in copious amounts of ^{13}C, subsequently burned radiatively during the AGB inter-pulse phase by $^{13}C(\alpha,\ n)^{16}O$. The neutrons released from this reaction drive the s-process. At low metallicity TDU is more efficient and there are many fewer iron-peak seed nuclei than at high metallicity. Consequently, the seed nuclei in the inter-shell region capture many neutrons at low metallicity, which enhances the production of heavy s-process nuclei relative to the lighter nuclei.

From Figure 3a of Busso et al. (2001), we estimate that the metallicity of the AGB stars responsible for the s–process enhancement in the metal–rich Sgr population was either [Fe/H] ≤ -1.6, or at a single, higher, metallicity, [Fe/H] ≈ -0.8 (due to the bi-valued nature of the heavy/light yield function), assuming the initial mass of the AGB stars is $\approx 1.5 M_\odot$ and the prescription for the mass of the ^{13}C pocket is the "standard value" divided by 1.5, which Busso et al. (2001) found best fits the observed composition of s-process enhanced stars.

It is significant that metal–rich, [Fe/H] ~ -0.1, stars are expected to produce [La/Y] $\approx -0.25 \pm 0.25$ (Busso et al. 2001); much lower than the observed value of [La/Y] $= +0.5$ dex. Therefore, the s–process enrichments in the metal–rich stars could not have been generated by the stars themselves, or produced by evolved companions. This observation also invalidates the instantaneous recycling assumption for the chemical evolution of the Sgr dSph.

Supporting evidence that these stars are not the products of self pollution comes from the fact that none of the metal–rich Sgr dSph stars are luminous enough to be on the thermally-pulsing AGB (TP-AGB). Our metal-rich Sgr sample have $2.5 \leq \log L/L_\odot \leq 2.9$, compared to the lowest TP-AGB onset luminosity of $\log L/L_\odot = 3.1$ from the calculations of Boothroyd & Sackmann (1988). Additional evidence against mass–transfer from an evolved companion comes from the frequency of such s–process enriched stars in the Galactic disk, at only 1 to 2% (MacConnell & Frye 1972). Thus, it is extremely unlikely that all the metal–rich Sgr dSph stars could have come from such a rare population.

The observation that all the metal–rich Sgr dSph stars show a similar enhancement in the ratio of heavy to light s–process elements, [La/Y] $\approx +0.45$, suggests that the progenitor AGB stars responsible for the s–process elements had [Fe/H] $\lesssim -1.6$**. Therefore, material from the metal–poor population must have been retained and**

recycled over timescales of many Gyr.

Our ages for the metal–rich Sgr dSph stars ([Fe/H] $\gtrsim -0.7$) range from ~ 0.5 to 3 Gyr, while the metal–poor stars range from ~ 3 to 12.5 Gyr; this is consistent with the expectation that metallicity smoothly increased with time (i.e., there were no accretion events mixing in large amounts of pristine gas on short timescales, which would have lowered the metallicity of the gas while leaving the element ratios unchanged) and that the most metal–poor population in the Sgr dSph are very similar to typical Galactic halo stars. The derived ages for the Sgr stars are in qualitative agreement with a period of extended star formation as indicated by the abundances of neutron-capture elements. A sophisticated chemical evolution model – incorporating inflow, outflow, non-instantaneous recycling, etc. – would be needed to fully test the qualitative agreement. Until we have better constraints on the star–formation history of the Sgr dSph, this will be left for future work; an unbiased metallicity function would be especially useful.

If our interpretation is correct, then these stars will show overabundances of lead and other heavy s-process elements. In addition the metal-rich Sgr stars should show no evidence of the short-lived element technitium if the s-process enhancements came from previous generations of AGB stars. It is clear that detailed chemical composition of the Sgr dSph stars, when combined with an accurate star–formation history for this galaxy, will provide useful constraints on s-process nucleosynthesis. In this regard, abundances of the diagnostic species rubidium and ^{96}Zr will be useful, as these are sensitive to details of the s-process conditions, which ultimately can constrain mass of the AGB progenitor and implicate an enrichment timescale.

We note that similar s–process enhancements have been seen in stars of the globular cluster Omega Centauri (e.g. Smith et al. 2000), but at lower metallicity; those enhancements were attributed to AGB nucleosynthesis by $M < 3\,M_\odot$ stars, whose lifetimes are ~ 0.3 Gyr (Girardi et al. 2000).

Similar s–process enhancements, accompanied by low α–element abundances have also been seen for stars in the Magellanic Clouds (e.g. Hill 1997). It seems that the Magellanic Clouds may have experienced a chemical evolution history similar to Sgr.

Our model for the evolution of the Sgr dSph is curiously opposite, in a sense, to the situation in the solar neighborhood. Near the Sun, the G–dwarf problem (van den Bergh 1962, Schmidt 1963; see Pagel 1997 for a thorough review of proposed solutions) is the observation that there are too few metal-poor stars to account for the high numbers of metal-rich stars under the assumption of simple, closed box, chemical evolution. Continuous inflow of lower or zero metallicity gas is the most favored way of solving the G-dwarf problem. Our model for the Sgr dSph requires a significant amount of outflow to explain the abundance patterns and the age–metallicity relationship. At the same time, we find that recycling of newly-synthesized elements operated over timescales of many Gyr because we believe the metal-poor population generated the elements that enriched the younger, more metal-rich, stars.

7.5. Comparison with Other Abundance Studies of Sgr dSph Stars

Including the chemical abundances found for M54 red giants (Brown, Wallerstein & Gonzales 1999; hereafter BWG99) and those of 2 Sgr dSph stars (Bonifacio et al. 2000; hereafter B00) strengthens the abundance trends we find in Sgr stars.

BWG99 derived chemical abundances for 5 red giant stars in the globular cluster M54, a member of the Sgr dSph, derived from CTIO 4m echelle spectra ($R \sim 24,000$; SNR ≈ 60). The stars were similar in color and magnitude to our three most metal–poor stars. BWG99 derived initial effective temperatures using (V–I) colors and the color–temperature relationships of Buser & Kurucz (1992). The reddening was assumed to be E(B–V) = 0.20 (higher than our assumed value of 0.13), in order to make their spectroscopic abundances derived from the Fe I and Fe II lines consistent. Gravities were computed assuming a mass of 0.7 $M_{\odot}$, and a short distance, at $(m - M)_V = 17.49$. An older set of model atmospheres from Bell et al. (1976) was used, but like us they assumed LTE analysis and used a version of MOOG for the abundance analysis. The line list was similar in size to our own, although the lines used differ.

The abundance ratios of the M54 stars are similar to our three most metal–poor stars. BWG99 note that the average abundance ratio [Ti/Fe] = +0.30 was somewhat higher than the average of their other α elements (Mg, Si, and Ca), at +0.16 dex. We do not find such a correlation for our metal-poor Sgr field stars. BWG99 detected Al in only one star, Ibata 1, and that star had such strong Al, [Al/Fe] = +0.78, accompanied by depleted O, [O/Fe] = −0.23, that they concluded its primordial abundance had been altered by proton-burning, similar to our star 1–73 as discussed in §7.3. We excluded Ibata 1 from the calculation of the average [Na/Fe] for M54 stars that is plotted in Figure 6, because the Na abundance also appears enhanced over primordial. BWG00 did not determine the abundance of Y, but the abundance ratios of the other neutron-capture elements follow the trends defined by our stars.

B00 derived chemical abundances for 2 field red giants in the Sgr dSph from high-dispersion spectra ($R \sim 43,000$; SNR ≈ 30) obtained with UVES on an ESO 8.2-meter telescope. The stars are somewhat hotter ($(V–I)_0 \approx 0.95$, $T_{eff} \approx 4900$ °K) and fainter (V = 18.2) than our sample. Effective temperatures were based on (V–I) colors and Alonso et al. (1999) color–temperature relationship, and gravities were assumed to be $\log g = 2.5$, consistent with the stars' positions in the color–magnitude diagram. Kurucz (1993) model atmospheres and LTE were assumed to derive abundances. The line list was different than used in the present work. The B00 spectra extend farther to the blue than ours, and cover some gaps in our spectra. However, our line list contains roughly double the number of lines for most of elements studied by B00. For example, for Ca and Fe we use 18 and 76 lines, respectively, while B00 use 6 and 16. However even though we use different line lists, we find very similar abundance results.

The derived metallicities of the B00 stars are [Fe/H] = −0.28 and −0.21, similar to our dominant group at high metallicity. The abundance ratios B00 derive fit very well onto the trends defined by our data, except that their [Fe/H] = −0.21 star has [α/Fe] = −0.16 which is lower by

~ 0.15 dex than the average value of our metal–rich stars, and their [Y/Fe] abundances are lower by ~ 0.3 dex than the average value of our metal–rich stars. Unfortunately, the four Y lines they used are all bluer than the limit of our spectral coverage so we cannot make a line-by-line comparison.

Since B00 detected 2 metal–rich stars in a dSph thought to be predominantly a metal-poor galaxy (recall Bellazzini et al.'s [1999] assertion that $\sim 85\%$ of the red giants were metal–poor based on their position in the color magnitude diagram, and an assumed age of ~ 15 Gyr) with unusual heavy element abundances, they were understandably confused about how to interpret their results. The stars had very similar atmospheric parameters and abundances, but their positions in the color–magnitude diagram were significantly different. In order to explain this, they discussed 5 hypotheses. They rejected photometric errors and differential reddening as the possible causes. Although they noted that an age difference of ~ 1 Gyr would explain the difference in photometry, they chose as the "most likely explanation" different distances for the stars and suggested the Sgr dSph had a non-negligible depth along the line of sight.

With many more stars in our sample, we find that a range in ages is the better explanation. An age range of ~ 1 to 13 Gyr, as inferred from our derived abundances and ages, is exactly what is needed to explain the trend in element ratios we see as a function of metallicity. B00 rejected the idea that the element ratios of the neutron capture were contaminated by the *s*–process in AGB stars because: (1) the stars were not luminous enough to have gone through thermal pulses that would contaminate their atmospheres, and (2) they rejected the idea that there was significant range in age of the stellar population of the Sgr dSph. B00 reached a different conclusion than we do simply because they had too small a sample to see the evolution of the element ratios with metallicity.

B00 noted that the unusual abundances found for the Sgr stars are very much like those seen in young supergiants in the Large and Small Magellanic Cloud (c.f., Hill 1997 and references therein). Therefore, our explanation of Sgr's unusual abundance variations – namely, slow evolution of the star–formation rate accompanied by mass loss and chemical enrichment of the young, metal–rich population by the old, metal–poor population – is probably applicable to the Magellanic Clouds. It is curious that the youngest stars in the Sgr dSph have approximately the same metallicities, as measured by [Fe/H], as the young stars in the LMC despite the fact that the total absolute magnitude, M_V, for the LMC is more than 5 magnitudes brighter than the Sgr dSph. Is this an artifact of star formation running to completion in Sgr dSph, or is it that much of Sgr's luminosity has already been stripped by tidal interactions with the Galaxy?

7.6. The Complex Evolution of the Sgr dSph

We can glean more information about the evolution of the Sgr dSph by comparing our data to some simple models. In Figure 13, we plot the age and [α/H] abundance, which is more likely to be a good candidate for the instantaneous recycling approximation than [Fe/H] because of the delayed

explosion of type Ia SNe which generate significant amounts of Fe but little α elements. For each of the globular clusters, we have assumed $[\alpha/\mathrm{Fe}] = +0.21$, which is the value found by BWG99 for M54, but the true value could be lower if its age is indeed 6 Gyr younger than the other clusters.

Figure 13 illustrates the results of simple outflow chemical evolution models with instantaneous recycling. For comparison, the models have all been normalized to pass through the same point. Each model assumes that star formation goes to completion at the present time of $T = 15$ Gyr, but adopts different prescriptions for the star–formation rate, $\psi(t)$. The black line shows the prediction assuming ψ is constant in time. Results for an exponentially decreasing star formation rate of the form $\psi(t) \propto e^{-t/\tau}$ are illustrated by the blue line for $\tau = 5$ Gyr and the green line for $\tau = 1$ Gyr. A model with an increasing star formation rate of the form $\psi \propto t$ is illustrated by the red line. Note that none of these simple outflow models accurately reproduces the observed age-metallicity relationship, but the sharp increase in $[\alpha/\mathrm{H}]$ for ages $\lesssim 5$ Gyr would imply an increasing, as opposed to decreasing, star formation rate. The most plausible model might well involve a discontinuous star–formation rate. Episodic star formation events have been found for a number of dSphs in the Local Group with the most stunning example being the Carina dSph (c.f., Hurley-Keller et al. 1998, Smecker-Hane & McWilliam 1999).

7.7. Relevance to the Merger History of the Galaxy

In §7.3 we introduced Fulbright's high-dispersion chemical abundance survey of 168 field stars in the solar neighborhood (Fulbright 2000). A detailed analysis of the kinematics of $\sim 45\%$ of these stars has been performed by Fulbright (2002). From such an extensive, homogeneous, database, strong constraints can be place on the merger history of the Galaxy by comparing the abundance ratios as a function of metallicity and kinematics to stars in dSph galaxies. In addition to our new data on 14 Sgr dSph stars, Shetrone, Côté & Sargent (2001; hereafter SCS01) have surveyed a total of 17 stars among the Ursa Minor, Draco and Sextans dSphs, also using HIRES. The philosophies of our programs are significantly different: we prefer to study many stars in one dSph to provide a detailed picture of the evolution of one galaxy, and we choose higher S/N data in order to analyze a larger set of chemical elements and always determine same set of elements in each star. SCS01 have obtained lower S/N data for a few stars in numerous dSphs with the primary goal of comparing the sum of the distribution to Galactic halo stars in order to constrain the merging history of the Galaxy. Even though the specifics of our two studies differ, they are extremely complimentary. Below we compare the composition of dSph stars with Fulbright's Galactic stars.

As mentioned in §7.3, Fulbright (2000) found a population of stars that have chemical peculiarities, $[\mathrm{Na/Fe}] < -0.2$ as opposed to the average of $[\mathrm{Na/Fe}] \approx 0$ for the majority of Galactic stars. In Figure 14 we show [Na/Fe] as a function of [Fe/H] for these stars as well as the dSph stars; Fulbright's "chemically–peculiar" stars are defined as those with $[\mathrm{Na/Fe}] < -0.2$. In the Fulbright sample, stars with [Na/Fe] deficits are also deficient in $[\alpha/\mathrm{Fe}]$, although by a smaller amount. This is exactly analogous to what we see in the metal–rich Sgr dSph stars. We have shown that the

smaller [α/Fe] deficits simply come from the fact that type Ia do produce some α–elements but very little Na. We suggest the *same* is true in Fulbright's chemically–peculiar stars. The proto-galactic fragments in which these stars formed apparently retained their individuality long enough for type Ia to explode in them and long enough for their nucleosynthetic products to cool and be recycled into new stars. Hence their star–formation activity must have lasted $\gtrsim 1$ Gyr, maybe more. The dSph stars show a mix of [Na/Fe] ratios. Some have [Na/Fe] roughly similar to normal Galactic halo stars while the majority show the same deficits in Na that the the chemically–peculiar halo stars and the metal–rich Sgr stars share. Therefore, we have evidence that even the lowest mass dSphs, Ursa Minor and Draco, underwent star formation on timescales $\gtrsim 1$ Gyr.

Fulbright (2002) shows that the majority of the chemically peculiar stars have very high Galactic rest frame velocities, > 300 km/s, and they are on very elliptical orbits, thus their kinematics suggest they could be the remnants of an outer halo, proto–galactic fragment(s).

We can actually place an upper-limit on the duration of their star formation by looking at the ratio of r and s–process elements. Again, the r–process is thought to primarily operate in massive stars that explode as type II SNe, so their enrichment happens quickly as opposed to the s–process enrichments, which may take on the order of a few Gyr or more. In Figure **??**, we plot the ratio of s–process to r–process elements as a function of metallicity. For the Fulbright and SCS01 stars, we plot the ratio [Ba/Eu], and for our Sgr dSph stars, we plot [La/Eu]. We do this because La was not measured in the Fulbright or SCS01 spectra, because at the lower metallicities, these lines can be very weak (e.g., Table 3). However, in our Sgr dSph spectra, the Ba lines for most stars are too strong for accurate abundance analysis, being on the flat portion of the curve of growth.

Examination of Figure **??** shows that only one of the Fulbright stars and one of the Ursa Minor dSph stars show much evidence for significant amounts of s–process material. Note that the Ursa Minor star is located right at the tip of the red giant branch and one wonders if it potentially has enriched itself or been enriched by mass transfer from a companion. CMDs of the Ursa Minor dSph show that most of its stars are very old, $\gtrsim 10$ Gyr (Hernandez, Gilmore, & Valls–Gabaud 2000, Dolphin 2002), and thus the timescale is such that self–pollution could be an issue. A point to note is that only a small subset of the Fulbright and SCS01 stars have measurements of La, Eu because the lines are weak in such metal-poor stars. Because of this, we caution that careful thought must be put into interpreting these diagrams. Selection effects could bias one's interpretation.

In Figure **??**, we show the same s to r–process ratios but as a function of the [Na/Fe] ratio. Stars enriched by Type Ia SNe will have [Na/Fe] below that of the normal yield of Type II SNe, [Na/Fe] ≈ 0. This diagram shows that there is no evidence for large amounts of s–process material in Fulbright's chemically–peculiar stars or in SCS01 stars, but again we really need more data on which to firmly base our conclusions because very few of these stars have measurements in La, Eu, Na and Fe. Therefore, we tentatively conclude that the SCS01 dSphs and the proto-galactic fragments that gave rise to the chemically–peculiar stars stopped forming their stars before the onset of significant enrichment from the s–process. Determining exactly what time that corresponds to will require

additional input from theoretical models, but we can compare to the Sgr dSph abundances and ages to get a hint. The $[s/r]$ ratios of the Fulbright stars are certainly lower than the metal-rich Sgr stars, the youngest of which is ~ 3 Gyr old, and thus formed ~ 12 Gyr after the initial epoch of star formation. Therefore, this is only a weak constraint in that the proto-galactic fragments and dSphs must have stopped forming stars > 3 Gyr ago.

8. Summary

Our observations of the Sgr dSph are consistent with prolonged star formation and chemical enrichment with significant mass loss. The radial velocities and chemical compositions firmly establish the 14 stars in our sample as bona fide Sgr dSph members with metallicities of $-1.6 \leq$ [Fe/H] ≤ 0.0 and an corresponding age range of ~ 13 to 1 Gyr.

While the composition of the metal–poor, [Fe/H] < -1, Sgr dSph stars closely resembles Galactic halo stars, the metal–rich component with $-0.6 \lesssim$ [Fe/H] $\lesssim 0$ shows a very unusual chemical composition: [Na/Fe] and [Al/Fe] ratios are on average 0.4 dex below those of stars with the same metallicity in the solar neighborhood while the $[\alpha/\mathrm{Fe}]$ ratios are only 0.1 dex below the solar neighborhood stars. From this we conclude the ratio of number of type II to type Ia SNe that enriched the metal-rich stars in the Sgr dSph was lower than that of stars in the solar neighborhood. These abundance ratios are consistent with ≈ 60 to 70% of the Fe in the metal-rich Sgr population synthesized in type Ia SNe and the remainder in type II SNe. Such abundance ratios could arise if the Sgr dSph experienced an episodic star-formation rate (meaning that star formation activity went through a lull between the formation of the Sgr metal-poor and Sgr metal-rich populations) or if the star–formation rate of the Sgr dSph proceeded at a steady pace but the pace was slower than that of the Galactic disk in the solar neighborhood.

Enhancements of neutron-capture heavy elements, which increase with [Fe/H] (up to [La/Fe]$\sim$1 dex at [Fe/H]$\sim$0), and the s–process signature seen in the [La/Eu] ratios, indicate the importance of AGB nucleosynthesis in the metal–rich Sgr dSph population. However, the [La/Y] ratios suggest a nucleosynthetic origin from sites of much lower metallicity than the stars themselves. These observations may be understood if heavy elements in the metal–rich population were dominated by input from low-mass, long-lived, AGB stars belonging to the old, metal–poor population. The relatively long-lived AGB progenitors require that star formation in Sgr dSph took place over an extended period of time, $\gtrsim 0.3$ to 2 Gyr if the initial mass of the AGB stars are ~ 3 to 1.5 $M_\odot$, respectively.

Finally, the increasing trend in [La/Fe] ratios to higher [Fe/H] indicates that either the efficiency of s-process production increased, or the production of iron decreased with time. The latter alternative strikes us as more likely, because the probability that mass transfer to a white dwarf will exceed the Chandrasekhar limit must be lower for a population of older, and hence less massive, secondaries.

These assertions are supported by age estimates for our sample of Sgr dSph stars, based on Padova isochrones, which span the range from 0.5 to 12.5 Gyr. The age-metallicity relationship for these Sgr field stars and the Sgr globular clusters suggest that the loss of gas in a galactic wind was very important in the evolution of this dSph. Thus we conclude that the Sgr dSph has had a surprisingly complex history of star formation and chemical enrichment.

We gratefully acknowledge financial support from the NSF through grants AST-9619460 and AST-0070895 to TSH, and AST-9618623 and AST-0098612 to AM. TSH also thanks the American Astronomical Society for a Small Research Grant that supported travel to Keck Observatory. We thank Rodrigo Ibata for sharing his radial velocities with us prior to their publication, and Inese Ivans for useful comments on the manuscript. We thank the staff at Keck Observatory for their excellent observing support, and Steve Vogt and collaborators for creating HIRES, an extremely reliable and efficient spectrograph. We thank Graeme Smith and Robert Kraft for agreeing to share nights in (what was then) an innovate scheduling arrangement. In addition, we want to extend special thanks to the people of Hawai'ian ancestry on whose sacred mountain, Mauna Kea, we were privileged to be guests. Our research was expedited by the wide range of data made available at Canadian Astronomy Data Center, which is part of the Herzberg Institute of Astrophysics, a facility of the National Research Council of Canada, the Digitized Sky Survey, which was produced at the Space Telescope Science Institute under US Government grant NAG W-2166, and the NASA Astrophysics Data System Abstract Service.

REFERENCES

Alonso, A., Arribas, S. & Martinez-Roger, C. 1999, A&AS, 140, 261

Alonso, A., Arribas, S. & Martinez-Roger, C. 2001, A&AS, 376, 1039

Arnesen, A., Bengtsson, A., Hallin, R., Lindskog, J., Nordling, C., & Noreland, T. 1977, Phys.Scripta 16, 31

Arnesen, A., Bengtsson, A., Hallin, R., Nordling, C., Staff, Ö. & Ward, L. 1981, Phys.Scripta 24, 747

Augason, G.C., Taylor, B.J., Strecker, D.W., Erikson, E.F. & Witteborn, F.C. 1980, ApJ, 235, 138

Bard, A., & Kock, M. 1994. A&A, 282, 1014

Bell, R.A., Eriksson, K., Gustafsson, B. & Norlund, A. 1976, A&AS, 23, 37

Bell, R.A. & Gustafsson, B. 1989, MNRAS, 236, 653

Blackwell, D.E., Ellis, R.S., Ibbetson, P.A., Petford, A.D. & Willis, R.B. 1975, MNRAS, 171, 425

Blackwell, D.E., Booth, A.J., Petford, A.D., Leggett, S.K., Mountain, A.J. & Selby, M.J. 1986, MNRAS, 221, 427

Blackwell, D.E., Petford, A.D., Arribas, S., Haddock, D.J. & Selby, M.J. 1990, A&A, 232, 396

Brown, J.A., Wallerstein, G., & Zucker, D. 1997, AJ, 114, 180

Brown, J.A., Wallerstein, G., & Gonzalez, G. 1999, AJ, 118, 1245

Bonifacio, P., Hill, V., Molaro, P., Pasquini, L., Di Marcantonio, P. & Santin, P. 2000, A&A, 359, 663 (B00)

Buser, R. & Kurucz, R.L. 1992, A&A, 264, 557

Busso, M., Gallino, R., & Wasserburg G.J. 1999, ARA&A, 37, 239

Busso, M. Gallino, R. Lambert, D.L., Travaglio, C. & Smith, V.V. 2001, ApJ, 557, 802

Bellazzini, M., Ferraro, F.R., & Buonanno, R. 1999, MNRAS, 307, 619

Bertelli, G., Bressan, A., Chiosi, C., Fagatto, F. & Nadi, E. 1994, A&AS, 106, 275

Boothroyd, A.I., & Sackmann, I.J. 1988, ApJ, 328, 653

Brown, J.A., Wallerstein, G. & Gonzalez, G. 1999, AJ, 118, 1245 (BWG99)

Burris, D.L., Pilachowski, C.A., Armandroff, T.E., Sneden, C., Cowan, J.J., & Roe, H. 2000, ApJ, 544, 302

Carney, B.W., Wright, J.S., Sneden, C., Laird, J.B., Aguilar, L.A., & Latham, D.W. 1997, AJ, 114, 363

Carretta, E., & Gratton, R.G. 1997, A&AS, 121, 95

Chen, Y.Q., Nissen, P.E., Zhao, G., Zhang, H.W., & Benoni, T. 2000, A&AS, 141, 491

D'Antona, F. 2001, in Extragalactic Star Clusters, IAU Symp. 207, eds. E. W. Grebel, D. Geisler & D. Minniti, (San Francisco: ASP), ASP Conf. Series (astro-ph/0105480)

Dohm-Palmer, R.C., Helmi, A., Morrison, H., Mateo, M., Olszewski, E.W., Harding, P., Freeman, K.C., Norris, J., & Schectman, S.A. 2001, ApJ, 555, 37

Dolphin, A. E. 2002, MNRAS, 332, 91

Edvardsson, B., Andersen, J., Gustafsson, B., Lambert, D.L., Nissen, P.E., & Tomkin, J. 1993, A&A, 275, 101

Fulbright, J.P. 2000, AJ, 120, 184

Fulbright, J.P. 2002, AJ, 123, 404

Gibson, B.K. 1998, ApJ, 501, 675

Gilmore, G., & Wyse, R.F.G. 1991, ApJ, 367, L55

Girardi, L., Bressan, A., Bertelli, G., & Chiosi, C. 2000, A&AS, 141, 371

Grebel, E. K. 2000, in *Star Formation from the Small to the Large Scale*, Proc. 33rd ESLAB Symp., ESA SP-445, eds. F. Favata, A. A. Kaas, & Wilson (Noordwijk: ESA), 87 (astro-ph/0007001)

Gratton, R.G., & Sneden, C. 1994, A&A, 287, 927

Green, E.M., Demarque, P., & King, C.R. *Yale Revised Isochrones and Luminosity Functions*, Yale University Observatory, New Haven, Connecticut, USA, 1987.

Grevesse, N., & Sauval, A.J. 1998, Space Science Reviews, 85, 161

Hannaford, P., Lowe, R.M., Grevesse, N., Biemont, E., & Whaling, W. 1982, ApJ 261, 736

Hernandez, X., Gilmore, G., & Valls-Gabaud, D. 2000, MNRAS, 317, 831

Hill, V. 1997, A&A, 324, 435

Hinkle, K., Wallace, L., Valenti, J., & Harmer, D. 2000, "Visible and Near Infrared Atlas of the Arcturus Spectrum 3727-9300 Å" ed. Kenneth Hinkle, Lloyd Wallace, Jeff Valenti, and Dianne Harmer. (San Francisco: ASP) ISBN: 1-58381-037-4, 2000.

Hurley-Keller, D., Mateo, M., & Nemec, J. 1998, AJ, 115, 1840

Ibata, R.A., Wyse, R.F.G., Gilmore, G., Irwin, M.J., & Suntzeff, N.B. 1997, AJ, 113, 634

Ivans, I.I., Sneden, C., Kraft, R.P., Suntzeff, N.B., Smith, V.V., Langer, G.E. & Fulbright, J.P. 1999, AJ, 118, 1273

Ivans, I.I., Kraft, R.P., Sneden, C., Smith, G.H., Rich, R.M. & Shetrone, M. 2001, AJ, 122, 1438

Iwamoto, K., Brachwitz, F., Nomoto, K., Kishimoto, N., Umeda, H., Hix, W.R., & Thielemann, F.K. 1999, ApJ, 125, 439

King, J.R. 1997, AJ, 113, 2302

Kraft, R.P., Sneden, C., Smith, G.H., & Shetrone, M.D. 1997, AJ, 113, 279

Kraft, R.P., & Ivans, I.I. 2003, PASP, 115, 143

Krebs, K. & Winkler, R. 1960, Z.Phys., 160, 320

Kubiak, M., McWilliam, A., Udalski, A., & Górski, K. 2002, Acta Astron., 52, 159

Kroupa, P. 2002, Science, 295, 82

Kurucz, R. L. 1988, Trans. IAU, XXB, M. McNally, ed., Dordrecht: Kluwer, 168

Kurucz, R.L. 1993, private communication

Lawler, J.E., Bonvallet, G. & Sneden, C. 2001, ApJ, 556, 452

Lawler, J.E., Wickliffe, M. E., den Hartog, E.A. & Sneden, C. (2001b) ApJ, 563, 1075

Layden, A.C., & Sarajedini, A. 2000, AJ, 119, 1760

MacConnell, D.J., & Frye, R.R. 1972, AJ, 77, 384

Malaney, R.A. 1987, ApJ, 321, 832

Mateo, M. 1996, in *Formation of the Galactic Halo ... Inside and Out*, eds. H. Morrison and A. Sarajedini, (San Francisco: ASP), ASP Conf. Series, 92, 434

Matteucci, F., & Brocato, E. 1990, ApJ, 365, 539

McWilliam, A. 1990, ApJS, 74, 1075

McWilliam, A. 1997, ARA&A, 35, 503

McWilliam, A., & Rich, R. M. 1994, ApJS, 91, 749 (MR94)

McWilliam, A., Preston, G.W., Sneden, C., & Shectman, S. 1995a, AJ, 109, 2736

McWilliam, A., Preston, G.W., Sneden, C., & Searle, L. 1995b, AJ, 109, 2757

Miller, G.E. & Scalo, J.M. 1979, ApJS, 41, 513

Newberg, H.J. et al. 2002, ApJ, 569, 245

Nissen, P.E., & Schuster, W.J. 1997, A&A, 326, 751

Pagel, B.E.J. 1997, *Nucleosynthesis and Chemical Evolution of Galaxies*, (Cambridge: CUP)

Pagel, B.E.J., & Patchett, B.E. 1975, MNRAS, 172, 13

Pardo, R.C., Couch, R.G., & Arnett, W.D. 1974, ApJ, 191, 711

Perrin, G., Coudé du Foresto, V., Ridgeway, S.T. et al. 1998, A&A, 331, 619.

Rich, R.M. 1990, ApJ, 362, 604

Rutledge, G.A., Hesser, J.E., & Stetson, P.B. 1997, PASP, 109, 907

Salaris, M., Chieffi, A., & Straniero, O. 1992, ApJ, 414, 580

Salaris, M., Cassisi, S., & Weiss, A. 2002, PASP, 114, 375

Salpeter, E.E. 1955, ApJ, 121, 161

Sarajedini, A., & Layden, A.C. 1995, 109, 1086 (SL95)

Scalo, J. 1986, Fund. of Cosmic Phys., 11, 1

Schmidt, M. 1963, ApJ, 137, 758

Sen, A. & Childs, W.J. 1987, Phys. Rev. A 36, 1983

Shetrone, M.D. 1996, AJ, 112, 1517

Shetrone, M.D., Côte, P., & Sargent, W.L.W. 2001, ApJ, 548, 592

Smecker-Hane, T. A., & McWilliam, A. 1999, in *Spectro-Photometric Dating of Stars and Galaxies*, eds. I. Hubeny, S. Heap & R. Cornett, (San Francisco: ASP), ASP Conf. Series, vol. 192, 150 (astro-ph/9910211)

Smith, V.V., Suntzeff, N.B., Cunha, K., Gallino, R., Busso, M., Lambert, D.L., & Straniero, O. 2000, AJ, 119, 1239

Sneden, C. 1973, ApJ, 184, 839

Sneden, C., Kraft, R.P., Shetrone, M.D., Smith, G.H., Langer, G.E., & Prosser, C.F. 1997, AJ, 114, 1964

Steenbock, W. 1985, in *Cool Stars With Excesses of Heavy Elements*, Proceedings of the Strasbourg Observatory Colloquium, Strasbourg, France, 1984, (Dordrecht: Reidel), 231

Steffen, M., & Holweger, H. 2002, å, 387, 258

Thévenin, F. & Idiart, T.P. 1999, ApJ, 521, 753

Thielemann, F.-K., Nomoto, K. & Yokoi, K. 1986, A&A, 158, 17

Travaglio, C., Galli, D., Gallino, R., Busso, M., Ferrini, F., & Straniero, O. 1999, ApJ, 521, 691

Udalski, A. 2003, ApJ, 590, 284

Unavane, M., Wyse, R.F.G., & Gilmore, G. 1996, MNRAS, 278, 727

van den Bergh, S. 1962, AJ, 67, 486

Vogt, S. S. et al. 1994, S.P.I.E., 2198, 362

Vogt, S. S. 1994, *HIRES User's Manual*, UCO/Lick Obs. Technical Report, No. 67

Wasserburg, G.J., Busso, M., & Gallino, R. 1996, ApJ, 466, L109

Wännström, A., Gough, D.S., & Hannaford, P. 1994, Z.Phys.D 29, 39

Wheeler, J.C., Sneden, C., & Truran, J.W. 1989, ARA&A, 27, 279

Winkler, H. 1997, MNRAS, 287, 481

Woolf, V.M., Tomkin, J. & Lambert, D.L., 1995, ApJ, 453, 660

Woosley, S.E. & Weaver, T.A. 1995, ApJS, 101, 181 (WW95)

Wyse, R.F.G., Gilmore, G., Houdashelt, M.L., Feltzing, S., Hebb, L., Gallagher, J.S. & Smecker-Hane, T.A 2002, New Astron., 7, 7, 395

Zinn, R., & West, M.J. 1984, ApJS, 55, 45

This preprint was prepared with the AAS LaTeX macros v5.0.

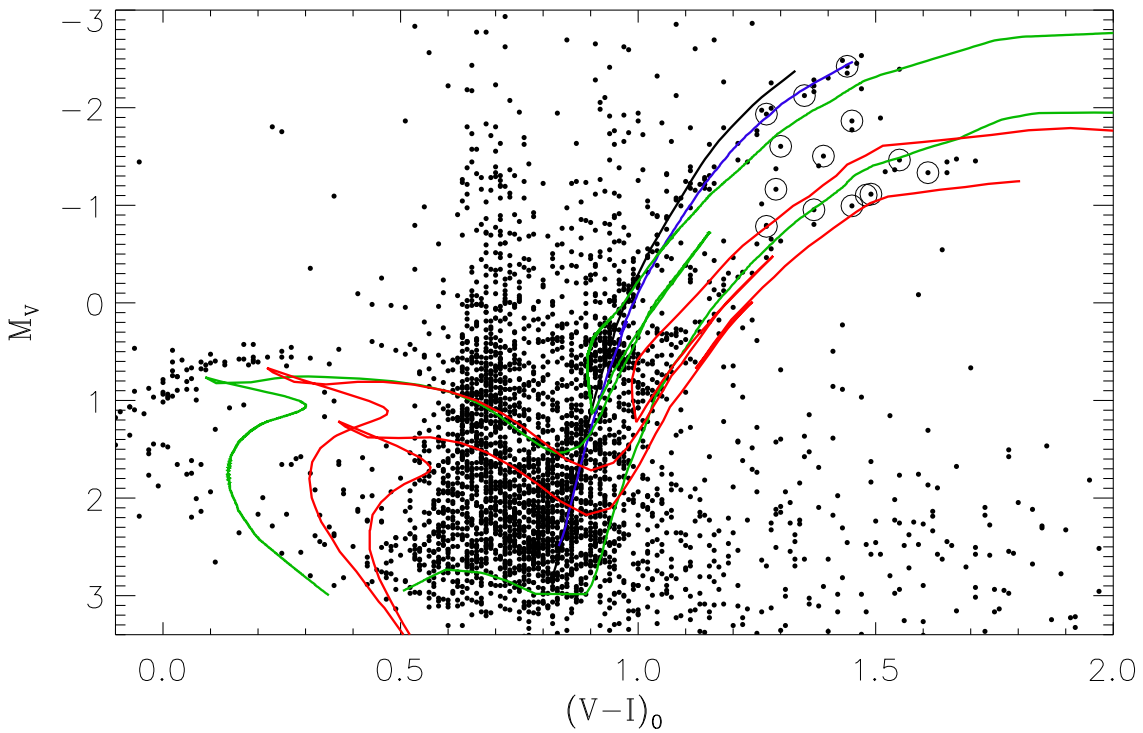

Fig. 1.— The color–magnitude diagram for the Sgr dSph (see text for details) with our spectroscopic targets shown as large circles. Our sample spans the full spread in color of red giant stars in order to probe the full range of metallicity. Isochrones based on the Padova models (Girardi et al. 2000) are shown as solid lines for a variety of age and metallicity combinations: black shows [Fe/H] = −1.4 and age = 13 Gyr, blue shows [Fe/H] = −1.0 and age = 5 Gyr, green shows [Fe/H] = −0.4 and ages = 1 and 3.5 Gyr, and red shows [Fe/H] = 0 and age = 1 and 1.4 Gyr. For the sake of clarity, evolutionary stages past the tip of the red giant branch are shown only for the two youngest models.

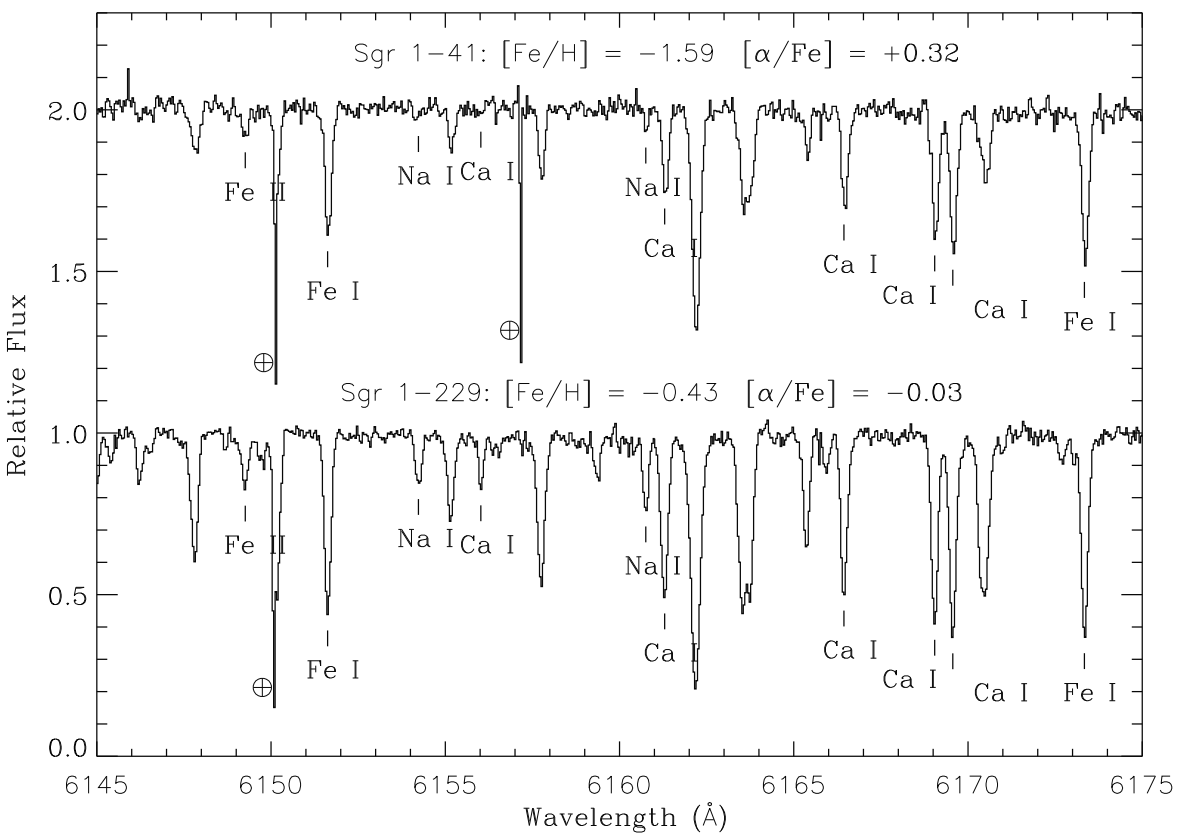

Fig. 2.— Spectra of a metal–poor (top) and metal–rich (bottom) Sgr dSph star. Spectra are shown redshifted to rest wavelengths, measured lines are labeled, and the derived metallicities are shown. Bad columns on the CCD are designated with the $\oplus$ symbol.

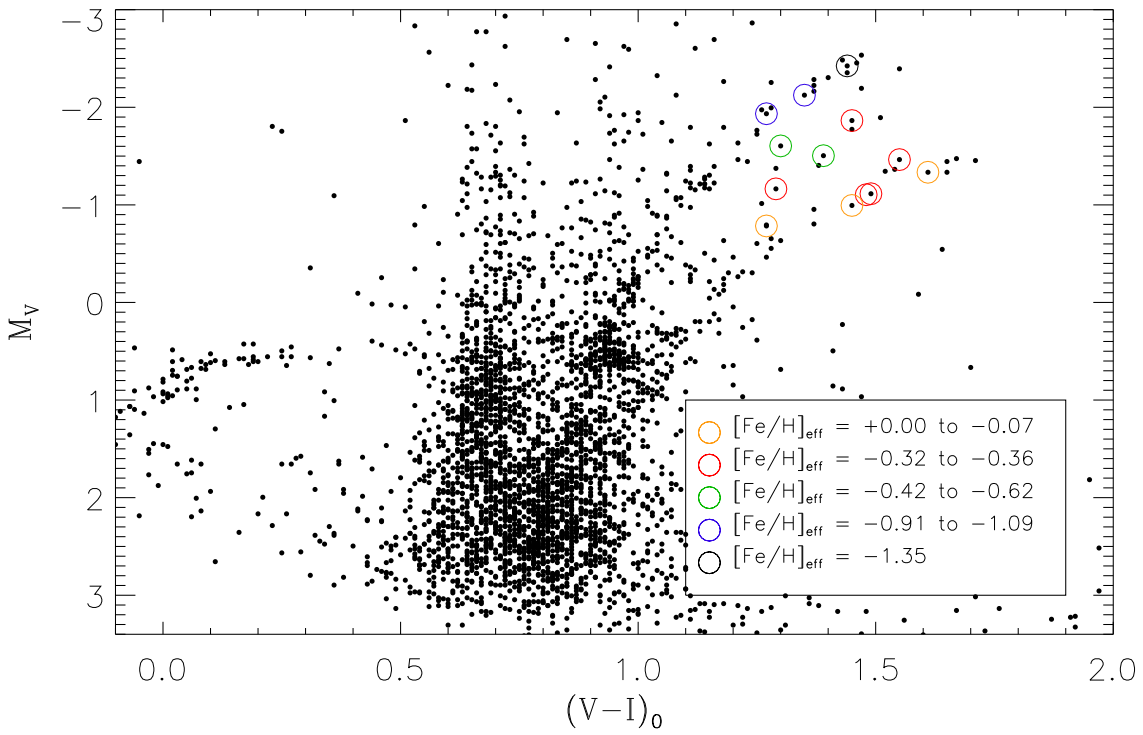

Fig. 3.— The color–magnitude diagram for the Sgr dSph (SL95) with stars in the spectroscopic sample circled in colors that reflect their derived effective metallicities (Eqn. 2).

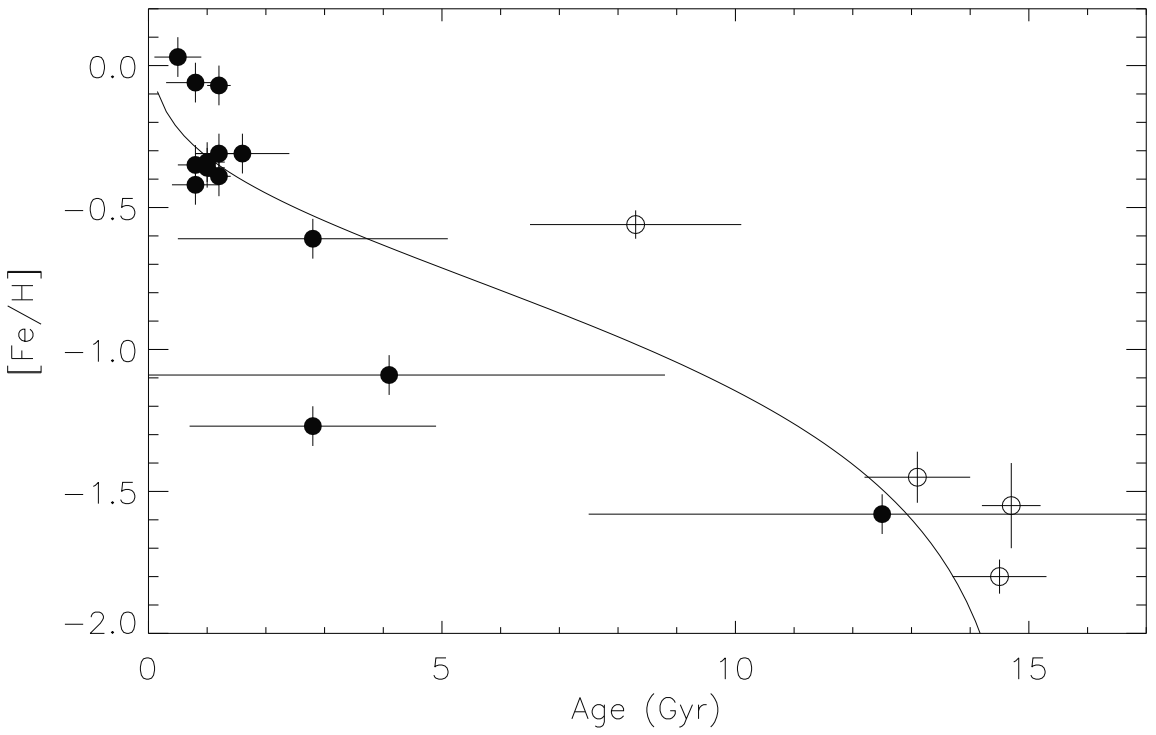

Fig. 4.— The age–[Fe/H] relationship for the Sgr dSph. Data for our red giant stars are shown as filled circles. Open circles show data for 4 globular clusters that belong to the Sgr dSph (see section 7.1 of the text for details). The solid line shows the prediction from a simple chemical evolution model that assumes instantaneous recycling, a closed box, star formation that has gone to completion at the present time.

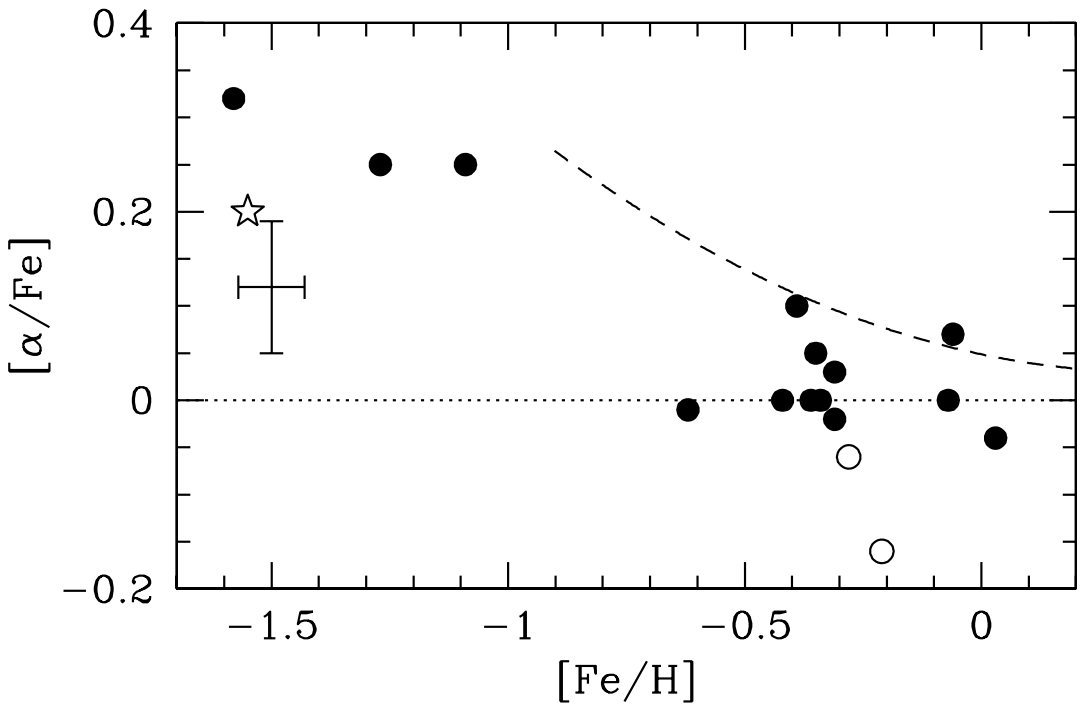

Fig. 5.— Chemical abundances for red giants in the Sgr dSph (filled circles), where [α/Fe] is the average of [Si/Fe], [Ca/Fe], and [Ti/Fe]. A typical error bar shown on the lower left. The average abundance of red giants in M54, a globular cluster in the Sgr dSph, from Brown, Wallerstein & Gonzalez (1999) is shown as the open star symbol. Sgr dSph stars for which Bonifacio, et al. (2000) derived abundances are shown as open circles. The dashed line represents the mean trend in [α/Fe] for stars in the solar neighborhood from Edvardsson et al. (1993).

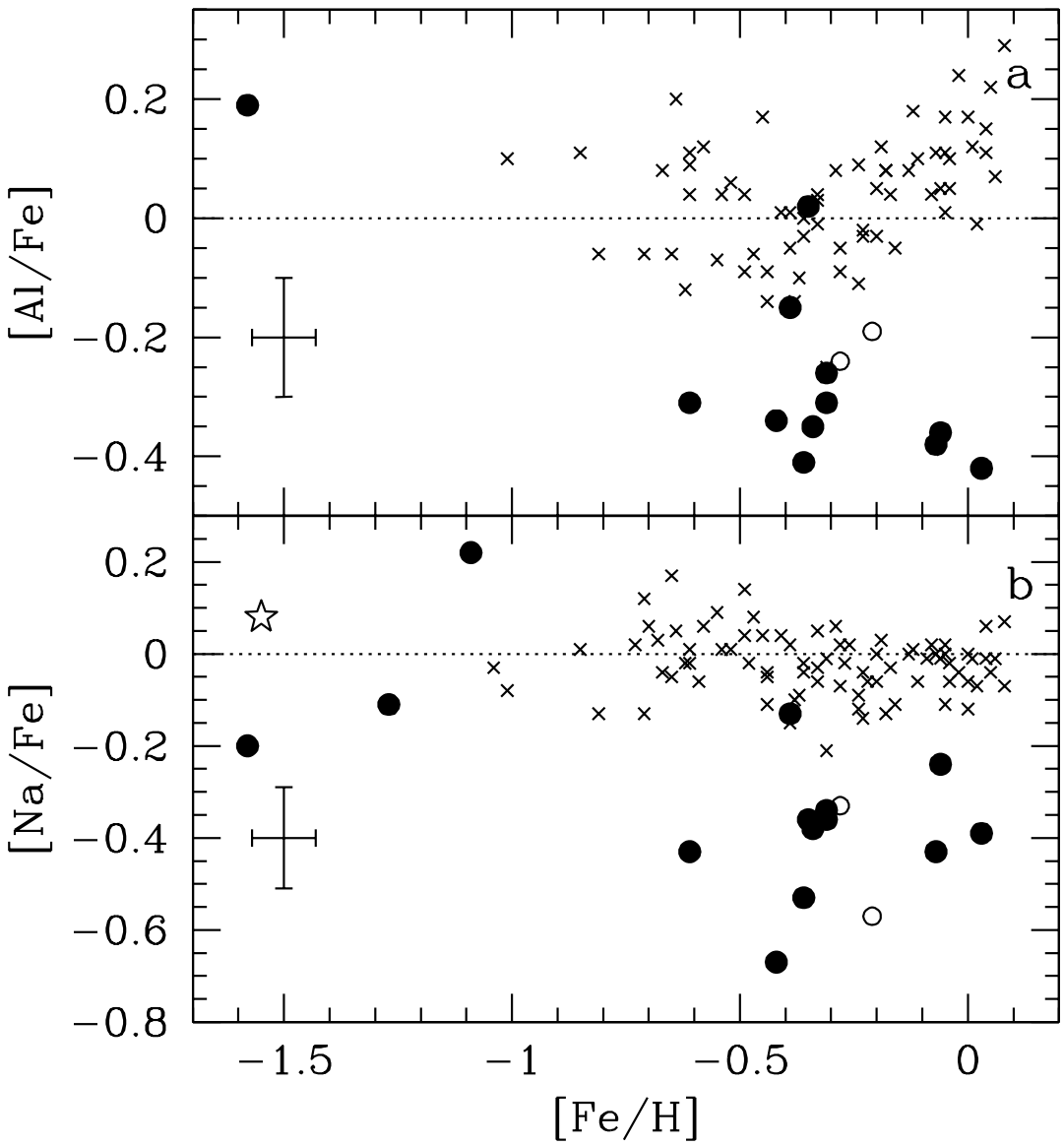

Fig. 6.— **a:** A plot of [Al/Fe] versus [Fe/H]. **b:** A plot of [Na/Fe] versus [Fe/H]. Symbols are the same as in Fig. 5. Crosses represent abundances from Chen et al. (2000) for solar neighborhood F stars.

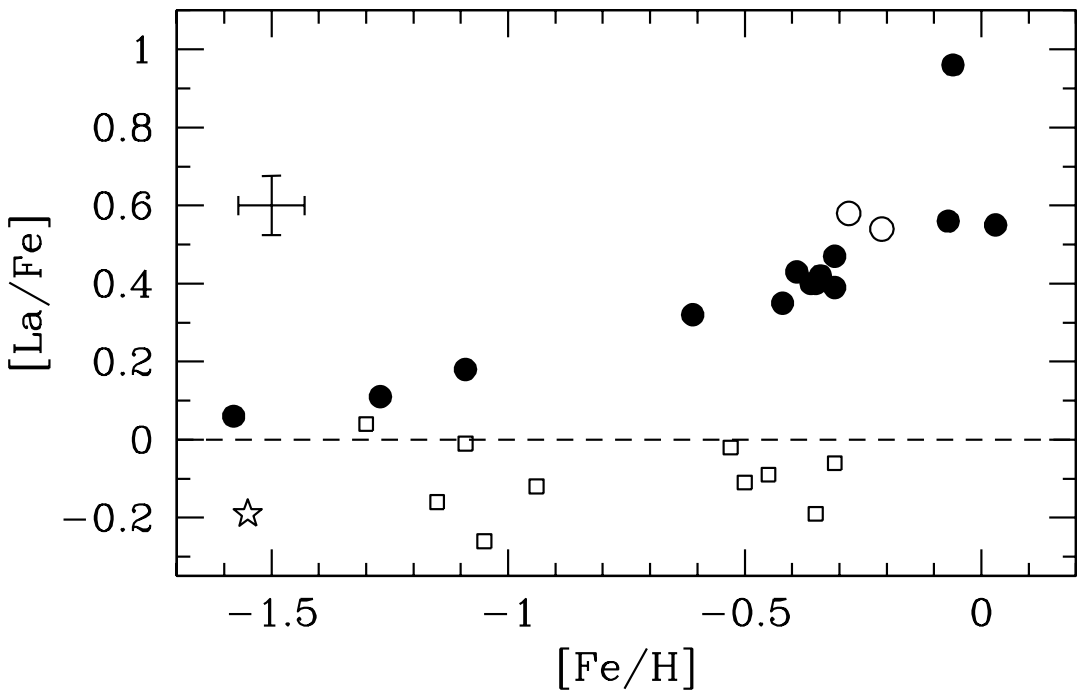

Fig. 7.— **a:** A plot of [La/Fe] versus [Fe/H]. Symbols are the same as in Fig. 5. Open squares represent chemical abundances of Galactic stars from Gratton & Sneden (1994).

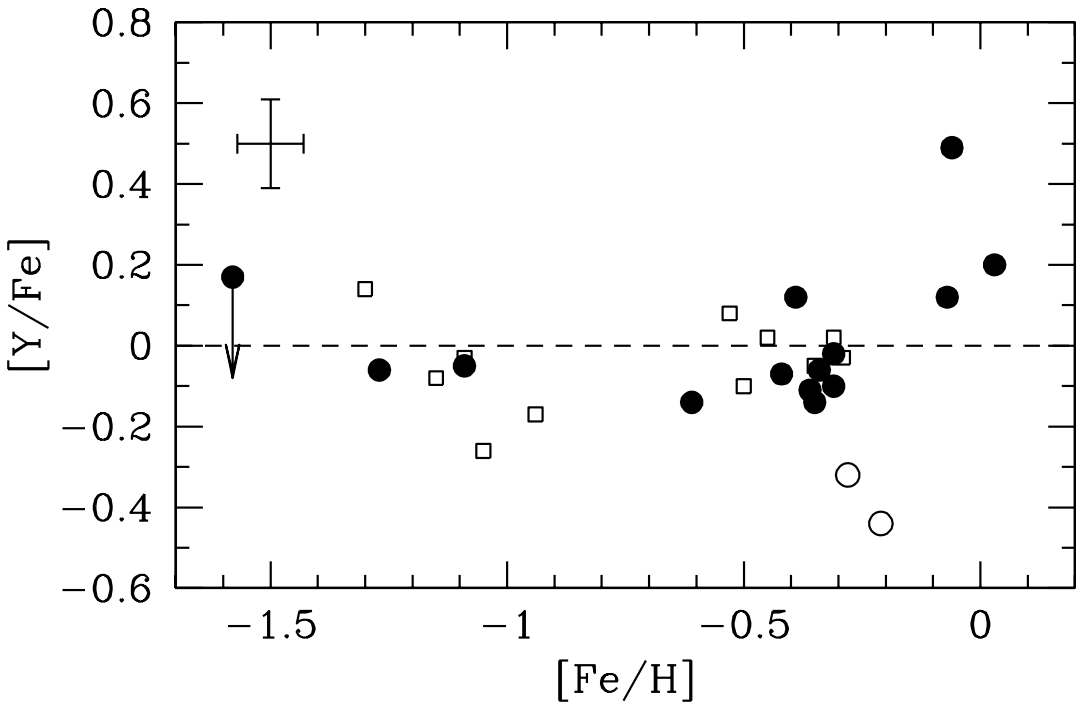

Fig. 8.— **a:** A plot of [Y/Fe] versus [Fe/H]. Symbols are the same as in Fig. 5. Open squares represent chemical abundances of Galactic stars from Gratton & Sneden (1994).

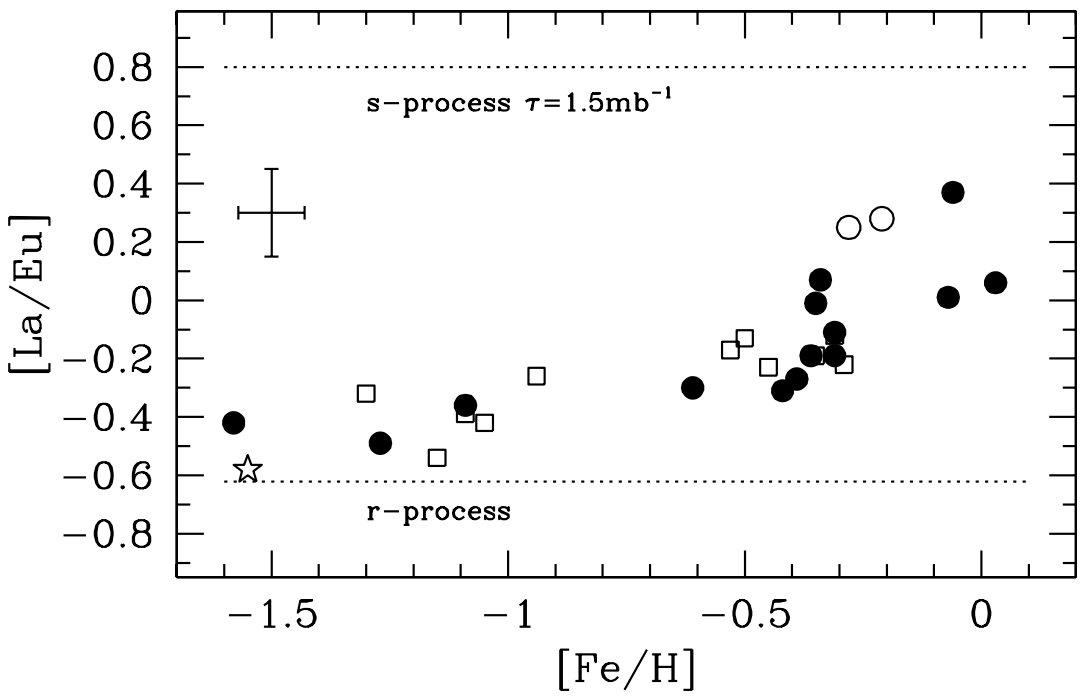

Fig. 9.— A plot of [La/Eu] versus [Fe/H]. Dotted lines indicate the solar r–process ratio, and a pure s–process ratio from Malaney (1987). Symbols are the same as in Fig. 5. Open squares represent chemical abundances of Galactic stars from Gratton & Sneden (1994).

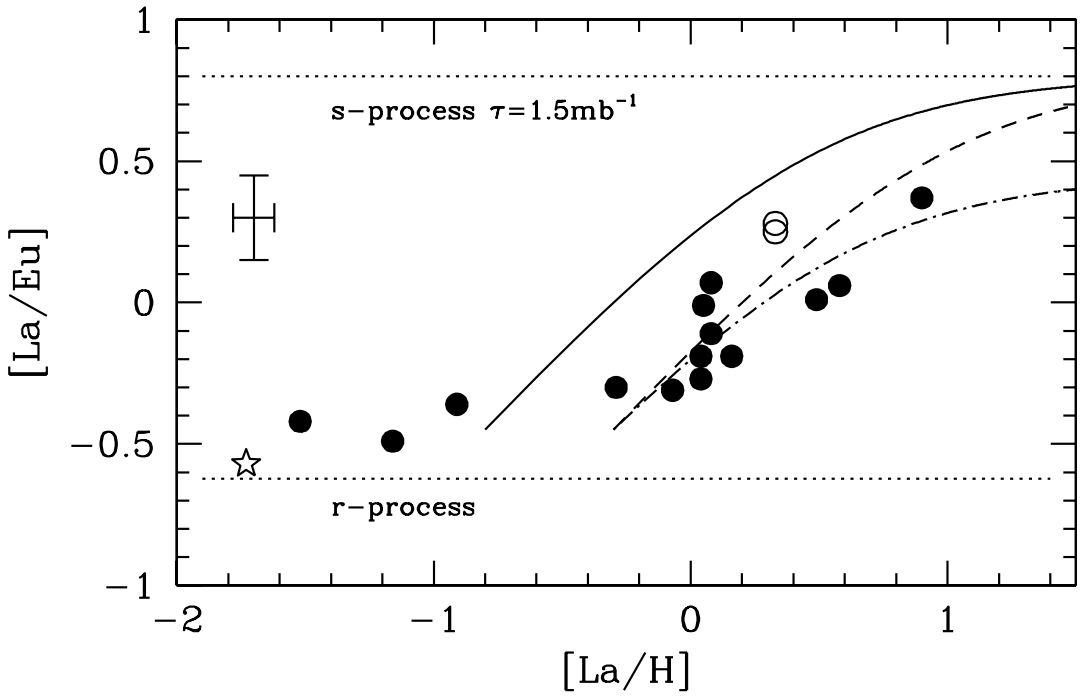

Fig. 10.— A plot of [La/Eu] versus [La/H]. Dotted lines indicate the solar r–process ratio, and a pure s–process ratio from Malaney (1987). Symbols are the same as in Fig. 5. The solid curve shows the composition locus of when pure s-process material is added to halo composition at [La/H]=−0.8, the dashed line shows the locus for pure s-process added to halo composition at [La/H]=−0.3, and the dot-dashed line shows the result of adding 95% s-process and 5% r-process composition to the halo mixture.

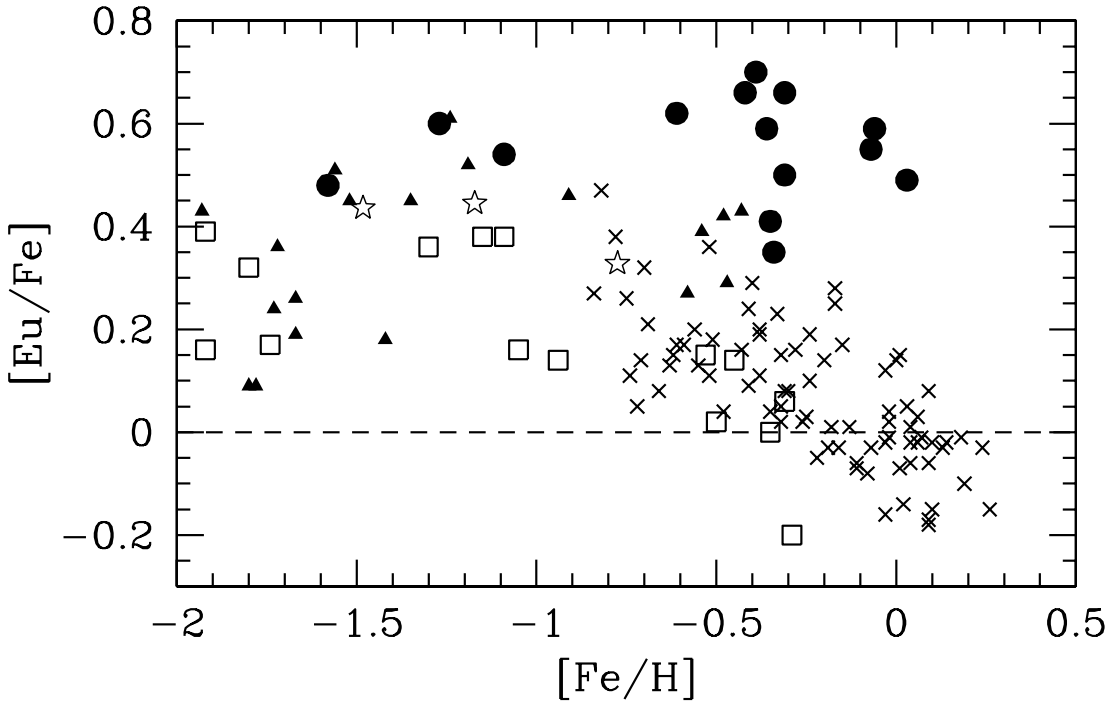

Fig. 11.— A plot of [Eu/Fe] versus [Fe/H] for the Sgr dSph stars (filled circles), compared with Galactic stars: crosses from Woolf et al. (1995); open squares from Gratton & Sneden (1994); open stars are Globular cluster mean values from Shetrone (1996); filled triangles are field halo stars from Shetrone (1996).

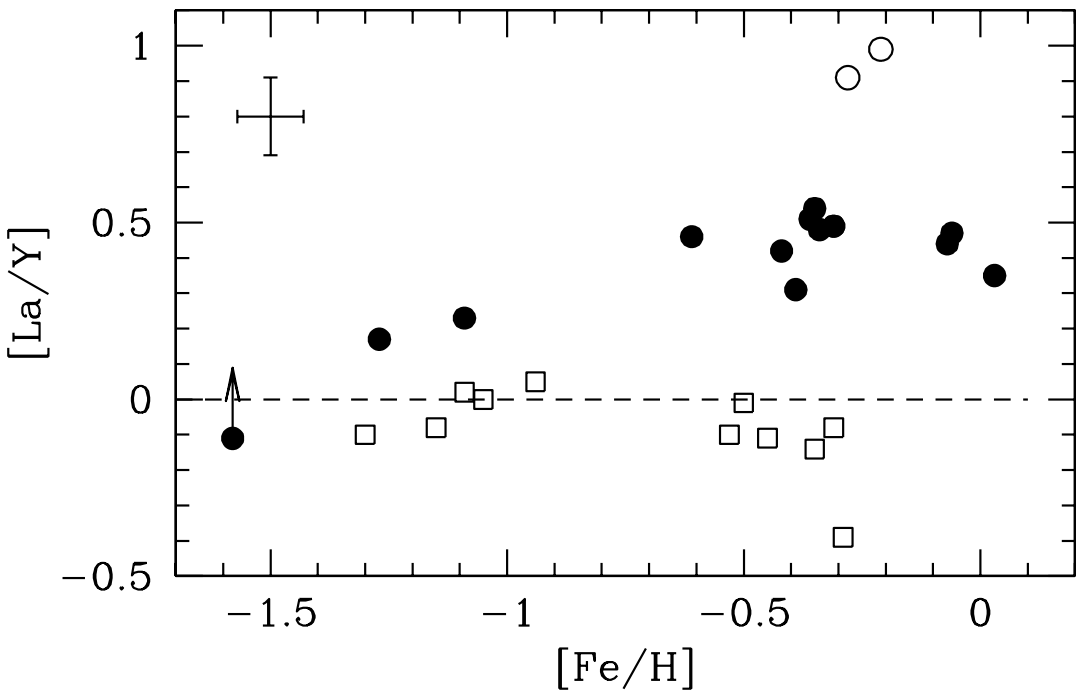

Fig. 12.— A plot of [La/Y] versus [Fe/H]. Symbols are the same as in Fig. 5. Open squares represent chemical abundances of Galactic stars from Gratton & Sneden (1994).

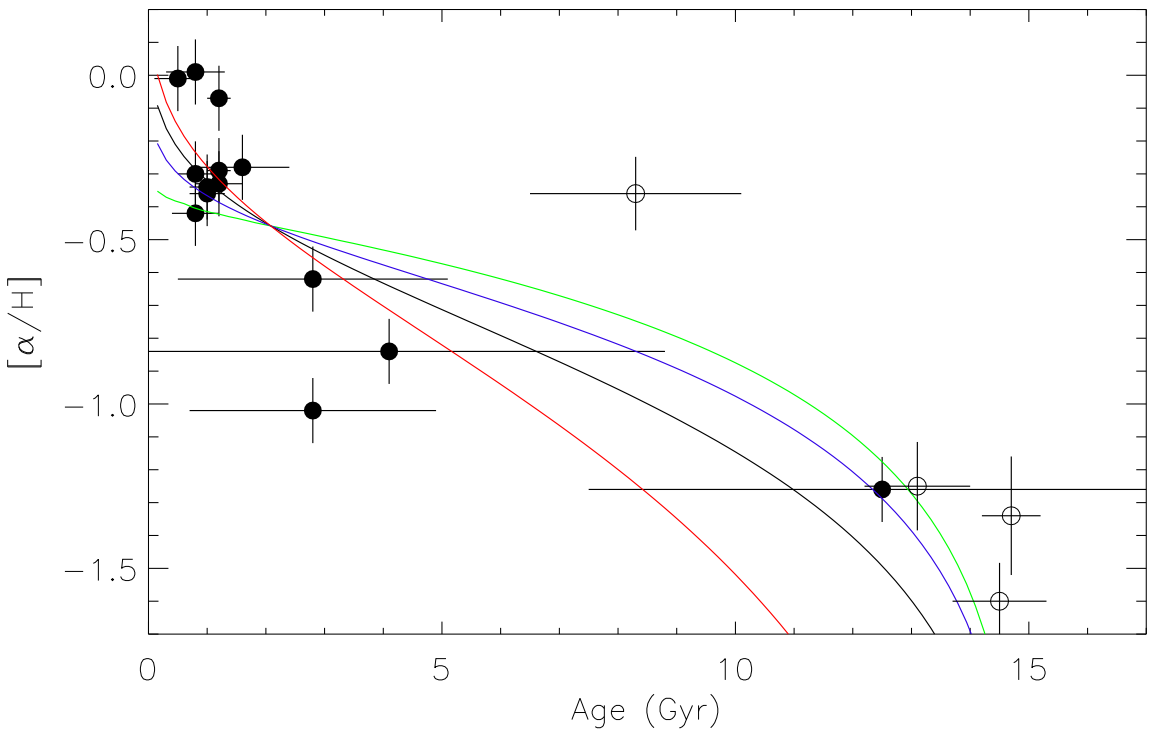

Fig. 13.— The age–metallicity relationship for the Sgr dSph. Filled circles show the data for our 14 red giant stars. Open circles show data for 4 globular clusters that are members of the Sgr dSph. Simple chemical evolution models that assume instantaneous recycling are shown as solid lines. See text in section 7.6 for details.

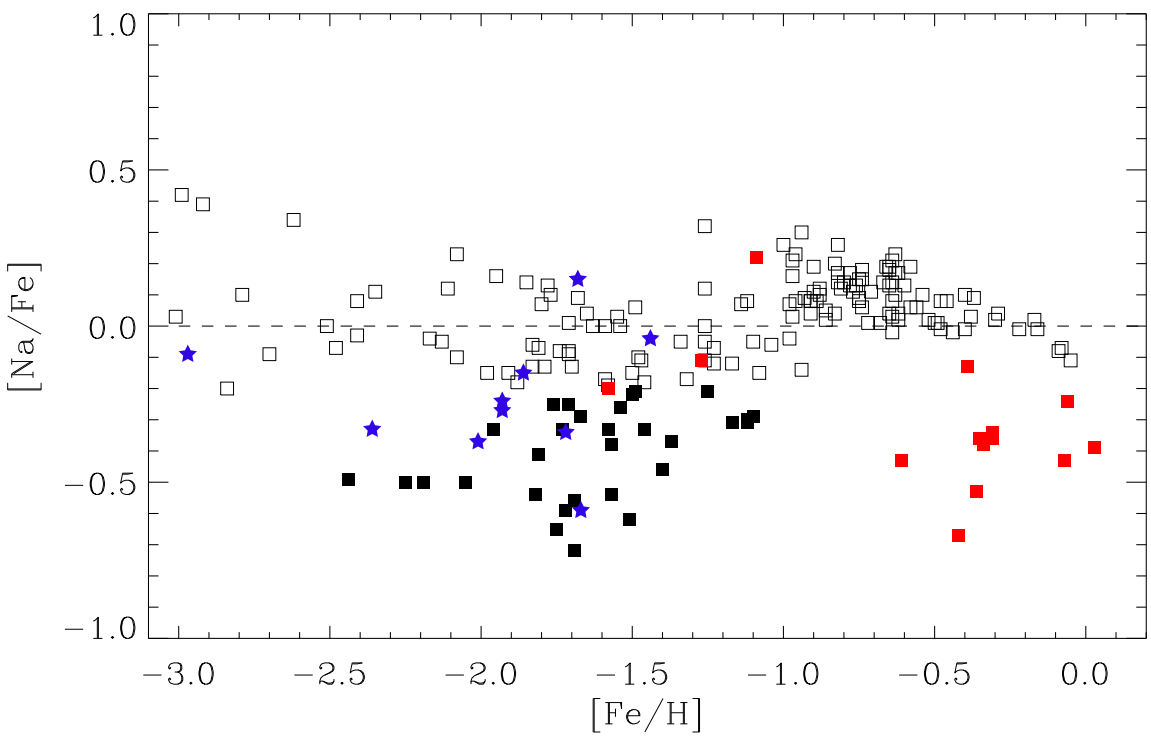

Fig. 14.— The ratio of [Na/Fe] as a function of [Fe/H] in dSph and Galactic stars. Sgr dSph stars from this paper are plotted as red squares. Stars in the Ursa Minor, Draco and Sextans dSphs from Shetone, Côté & Sargent (2001) are plotted as blue stars. Galactic stars in the Fulbright (2000) sample that have [Na/Fe] < -0.2 are plotted as black squares while those with [Na/Fe] ≥ -0.2 are plotted as open squares.

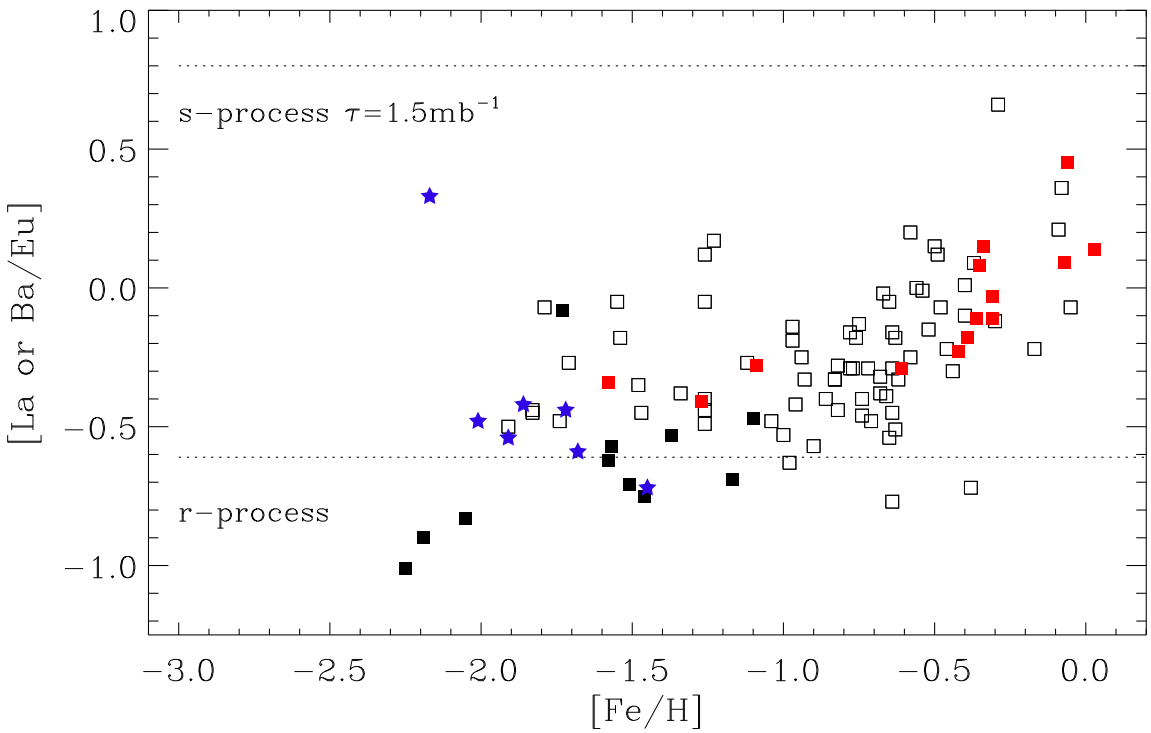

Fig. 15.— The ratio of s–process to r–process elements, [La/Eu] for Sgr stars or [Ba/Eu] for other dSph or Galactic stars, as a function of metallicity. Symbols are the same as Figure 14.

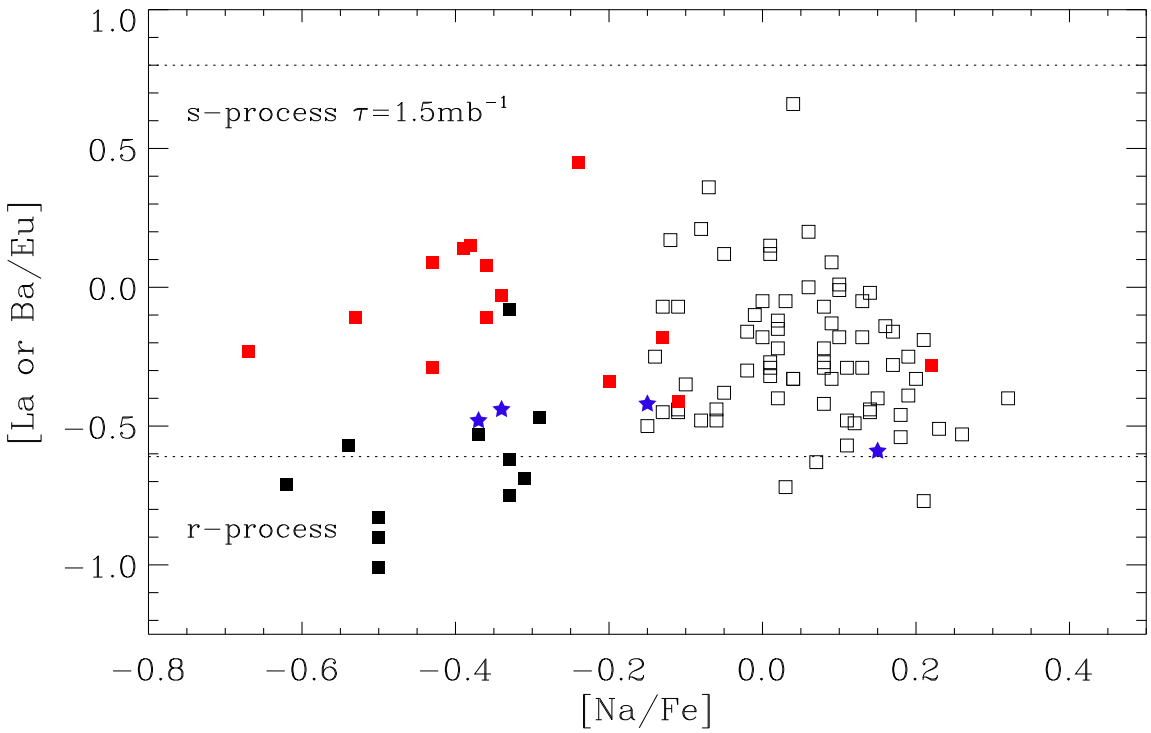

Fig. 16.— The ratio of s–process to r–process elements, [La/Eu] for Sgr stars or [Ba/Eu] for other dSph or Galactic stars, as a function of [Na/Fe]. Same symbols as Figure 14.

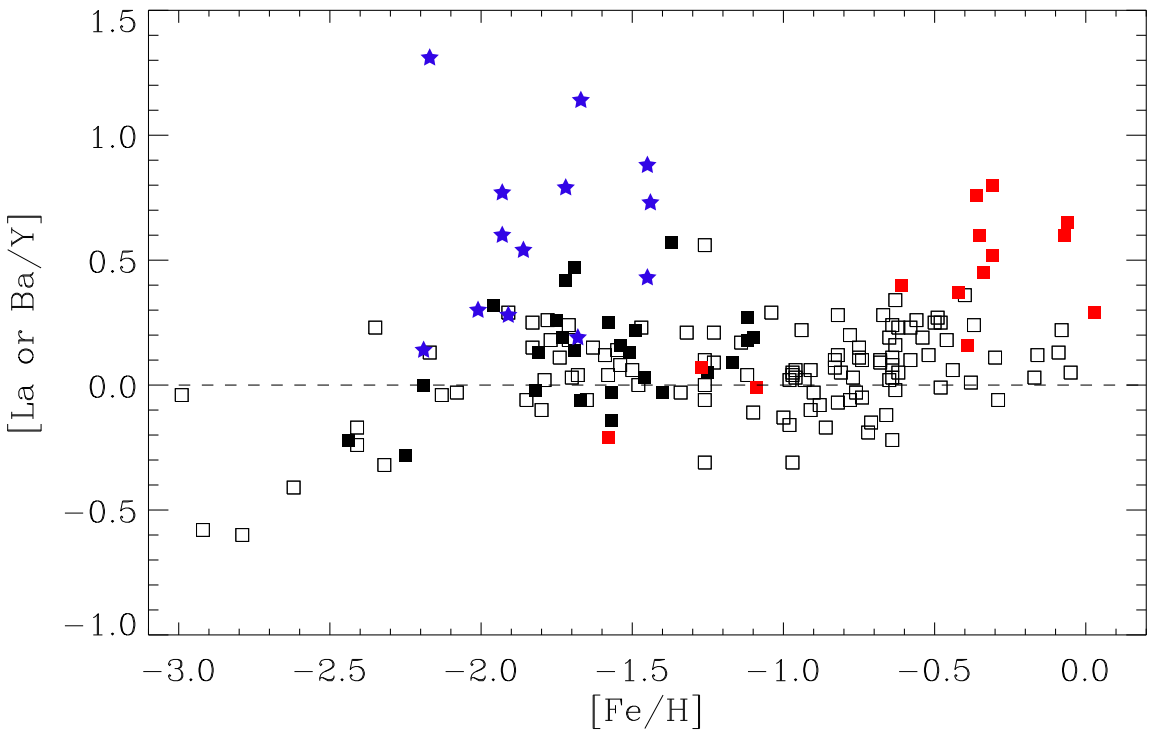

Fig. 17.— The ratio of heavy to light *s*–process elements, [La/Y] for Sgr stars or [Ba/Y] for other dSph or Galactic stars, as a function of metallicity. Same symbols as Figure 14.

Table 1. Stellar Coordinates and Photometry

Star	α(J2000)	δ(J2000)	K	$\sigma_{\rm K}$	J–K	$\sigma_{\rm J-K}$	V	$\sigma_{\rm V}$	V–I	$\sigma_{\rm V-I}$
1–41	18:55:13.55	−30:26:04.4	11.561	0.014	0.911	0.038	15.23	0.007	1.62	0.006
1–73	18:55:14.14	−30:28:54.9	11.845	0.017	0.952	0.034	15.53	0.001	1.53	0.005
1–87	18:55:11.88	−30:27:24.0	12.335	0.053	0.906	0.068	15.72	0.004	1.45	0.005
1–95	18:54:48.67	−30:31:29.8	12.021	0.019	0.973	0.043	15.79	0.006	1.63	0.003
1–229	18:55:09.40	−30:32:32.5	13.075	0.032	0.913	0.057	16.49	0.007	1.47	0.007
1–242	18:54:49.60	−30:31:33.7	12.713	0.016	1.014	0.043	16.54	0.008	1.67	0.003
1–150	18:54:44.70	−30:26:17.0	12.502	0.029	0.960	0.051	16.15	0.007	1.57	0.008
1–245	18:55:09.58	−30:29:16.9	12.731	0.017	0.927	0.049	16.55	0.004	1.66	0.002
1–267	18:54:55.87	−30:26:46.3	12.898	0.019	0.978	0.052	16.66	0.008	1.63	0.005
2–38	18:54:53.33	−30:14:51.5	12.550	0.022	0.930	0.048	16.05	0.001	1.48	0.002
2–44	18:55:10.91	−30:19:49.3	12.224	0.013	0.984	0.027	16.19	0.001	1.73	0.004
2–52	18:55:06.62	−30:15:48.7	12.240	0.020	1.004	0.056	16.32	0.004	1.79	0.003
2–75	18:54:47.23	−30:18:53.0	13.092	0.021	0.981	0.034	16.70	0.002	1.55	0.004
2–85	18:54:47.20	−30:16:08.0	13.515	0.023	0.812	0.062	16.87	0.003	1.45	0.006

Table 2. Journal of Observations

Star	UT Date of Observing Run	Exposure Time (sec)	SNR (6620Å)	$v_{\rm helio}$ (km/s)
1–41	22–24 August, 1996	1260	33	147.2
〃	10 July, 1997	3200	50	146.0
1–73	10–11 August, 1997	6320	70	139.4
1–87	10–11 August, 1997	6200	61	145.2
1–95	19–20 August, 1998	5400	44	143.4
1–150	23–24 July, 1998	9000	68	129.7
1–229	23–24 July, 1998	9000	57	153.2
1–242	19–20 August, 1998	9000	60	146.7
1–245	19–20 August, 1998	7020	35	138.1
1–267	19–20 August, 1998	9000	43	145.2
2–38	23–24 July, 1998	7200	56	130.4
2–44	22–24 August, 1996	7200	56	139.1
〃	10 July, 1997	4700	29	138.7
2–52	22–24 August, 1996	7200	57	154.2
〃	10 July, 1997	8500	38	154.4
2–75	10–11 August, 1997	10500	49	144.4
2–85	10–11 August, 1997	10800	46	154.1

Table 3. Equivalent Widths

Ion	Wavelength (Å)	Star 1–41	Star 1–73	Star 1–87	Star 1–95	Star 1–150	Star 1–229	Star 1–242	Star 1–245	Star 1–267	Star 2–38	Star 2–44	Star 2–52	Star 2–75	Star 2–85
Na I	5682.65	36	...	...	123	85	122:	137	98	115	112:	131	142	143:	...
Na I	6154.23	...	51	17	69	35	39	67	43	72	28	77	86	61	69
Na I	6160.75	14	66	17	88	62	52	87	58	104	43	99	127	80	98
Al I	5557.07	...	...	...	35	22:	...	...	...	...	20:	30	...	...	...
Al I	6696.03	18	115	...	67	46	44	70	61	89	41	85	85	71	73
Al I	6698.67	9	82	...	47	29	28	42	55	48	25	40	64	41	47
Si I	5690.43	28	...	...	...	49	58	65	72	71	48	77	68	51	...
Si I	6237.33	17	43	27	52	41	48	65	55	63	38	45	78	48	64
Si I	6721.84	16	36	...	43	24	34	48	...	51	27	...	74	37	59
Si I	6976.50	...	20	18	...	28	30	29	...	38	31	...	30	33	52
Si I	7235.33	18	27	18	36	23	32	28	38	...	10:	25	22	34	44
Si I	7405.79	46	87	43	84	68	81	81	66	86	70	75	78	66	89
Si I	7415.96	42	78	39	76	62	94	79	80	79	74	64	79	79	95
Si I	7423.51	59	64	54	49	70	87	80	90	88	87	70	76	89	94
Ca I	5260.39	...	43	40	84	77	70	82	80	92	68	106	112	74	88
Ca I	5581.98	129	...	...	209	138	170	192	...	196	153	...	213	...	...
Ca I	5588.76	148	...	...	242	189	197	214	162	223	198	211	243	202	...
Ca I	5590.13	94	...	...	169	137	136	164	137	154	131	151	157	146	...
Ca I	5867.57	21	37	18	69	58	50	77	67	92	57	100	95	70	81
Ca I	6156.02	...	21	18	65	35	31	50	41	73	34	57	74	57	61
Ca I	6161.30	64	...	...	163	132	127	157	140	164	134	166	223	147	...
Ca I	6166.44	75	96	76	137	130	114	132	121	144	98	143	157	127	138
Ca I	6169.04	99	126	99	168	139	139	162	141	173	144	171	196	152	155
Ca I	6169.56	116	144	110	189	162	154	180	148	188	163	194	210	170	195
Ca I	6449.82	114	143	110	162	146	161	174	147	171	147	185	228	163	183
Ca I	6455.61	60	98	61	126	108	106	129	121	140	114	137	156	118	134
Ca I	6471.67	117	138	117	170	146	149	169	179	180	148	179	186	176	168
Ca I	6493.79	142	158	131	204	175	170	204	169	207	174	200	210	196	195
Ca I	6508.85	...	19	8	58	35	40	64	48	73	38	66	97	56	71
Ca I	6572.80	114	159	105	244	201	182	262	182	270	195	276	317	230	237
Ca I	7148.15	154	180	147	217	198	196	209	199	226	195	214	240	200	229
Ca I	7326.16	97	131	106	189	151	144	171	...	191	157	202	207	172	183
Ti I	5223.63	...	51	38	90	80	79	112	65	115	64	128	135	102	98
Ti I	5282.40	...	...	...	...	96	...	...	...	...	86	...	162	116	...
Ti I	5295.78	52	81	58	129	99	95	134	85	128	91	113	148	113	96
Ti I	5384.63	...	31	15	72	52	38	86	36	93	40	95	101	76	62
Ti I	5436.70	...	...	...	126	39	82	14	39	91	47	...	197	...	...
Ti I	5453.65	...	48	...	...	75	60	...	57	...	67	112	132	...	98
Ti I	5471.21	34	59	27	109	82	81	112	78	113	...	122	128	101	102
Ti I	5474.23	41	72	32	147	96	78	125	104	122	76	113	139	99	106
Ti I	5503.90	...	39	24	107	67	69	103	56	114	49	107	112	90	80
Ti I	5648.57	21	34	21	77	60	53	91	61	92	52	100	106	78	84
Ti I	6743.13	85	119	61	173	147	115	194	122	182	131	183	213	145	164
Ti I	6861.45	16	35	18	88	57	44	75	43	82	47	86	102	64	70

Table 3—Continued

Ion	Wavelength (Å)	Star 1–41	Star 1–73	Star 1–87	Star 1–95	Star 1–150	Star 1–229	Star 1–242	Star 1–245	Star 1–267	Star 2–38	Star 2–44	Star 2–52	Star 2–75	Star 2–85
Ti I	7251.72	89	125	79	172	137	142	185	121	188	135	184	205	159	162
Ti II	5226.55	...	135	133	170	158	172	170	152	229	163	163	223	...	174
Ti II	5336.78	130	129	108	136	136	124	140	118	135	135	132	142	117	117
Ti II	6606.98	22	...	...	47	33	39	46	31	39	30	50	...	36	...
Fe I	6151.62	93	106	93	146	137	136	156	129	153	103	...	...	131	129
Fe I	6173.34	125	139	122	173	155	155	181	146	169	153	...	...	161	152
Fe I	6180.21	83	101	81	145	129	128	144	...	144	131	145	145	138	141
Fe I	6188.00	39	60	37	108	84	87	91	97	...	91	101	97	89	102
Fe I	6219.29	149	163	126	201	177	181	206	168	189	174	...	...	169	199
Fe I	6229.23	52	71	43	124	98	105	117	...	...	85	123	122	108	129
Fe I	6240.65	90	111	86	141	127	127	152	132	147	123	...	136	139	128
Fe I	6246.33	117	133	110	156	148	145	173	156	159	160	...	...	156	152
Fe I	6270.23	75	100	67	129	118	109	145	119	124	119	123	132	114	121
Fe I	6271.28	22	42	21	76	70	72	...	65	...	72	83	105	80	92
Fe I	6297.80	135	143	107	190	159	165	202	163	197	168	...	...	160	172
Fe I	6335.34	...	173	137	238	198	195	239	204	243	204	...	...	184	218
Fe I	6336.83	102	123	104	163	136	143	159	158	170	147	...	...	133	165
Fe I	6353.85	...	35	13	79	53	44	77	51	71	47	79	86	55	69
Fe I	6355.04	106	128	93	183	151	167	189	...	185	159	...	...	158	140
Fe I	6380.75	36	72	36	103	81	84	97	76	103	86	94	116	89	107
Fe I	6392.54	41	58	34	100	85	90	101	79	107	74	110	106	85	90
Fe I	6393.61	...	192	154	265	225	229	278	220	257	138	...	...	239	230
Fe I	6411.66	129	141	116	182	159	154	181	162	172	169	...	...	175	164
Fe I	6475.63	87	112	88	143	124	129	148	133	147	121	137	...	131	146
Fe I	6481.88	111	133	111	169	151	153	177	148	173	144	...	...	151	158
Fe I	6494.99	...	234	185	289	263	261	325	251	314	262	...	...	277	309
Fe I	6498.95	126	158	116	201	169	170	217	161	208	171	...	...	177	191
Fe I	6518.37	81	92	72	131	119	123	141	113	142	131	131	136	117	135
Fe I	6591.31	...	...	9	...	...	36	...	...	...	32	...	...	...	58
Fe I	6593.87	140	138	124	207	170	178	201	167	190	175	...	...	178	207
Fe I	6597.57	...	35	22	71	64	59	71	61	66	54	66	75	63	76
Fe I	6608.04	38	61	39	113	92	91	116	60	110	80	119	113	95	108
Fe I	6627.56	...	29	17	59	44	51	59	50	66	61	60	72	56	65
Fe I	6646.97	23	...	22	76	67	55	77	51	72	56	73	90	70	76
Fe I	6648.12	38	89	35	125	85	85	113	87	108	73	127	125	110	113
Fe I	6699.14	...	13	...	22	17	18	25	29	31	24		32	21	31
Fe I	6703.58	55	75	52	119	98	108	107	101	119	92	115	119	102	112
Fe I	6704.50	...	...	9	27	18	19	27	22	35	21	27	38	21	43
Fe I	6705.11	24	46	33	82	67	64	77	70	81	63	78	74	78	97
Fe I	6710.32	58	90	60	129	107	106	135	107	125	95	123	135	109	118
Fe I	6713.75	...	20	13	52	37	37	46	35	46	35	45	48	43	49
Fe I	6715.39	...	...	16	67	47	51	70	56	74	57	69	...	71	79
Fe I	6716.25	...	...	10	...	32	37	40	...	...	34	47	...	46	64
Fe I	6725.36	...	19	15	52	48	50	64	43	60	42	59	68	53	66
Fe I	6726.67	25	42	31	81	65	71	72	68	76	65	70	68	74	87
Fe I	6733.15	...	26	14	55	45	42	58	53	63	45	65	63	46	65

Table 3—Continued

Ion	Wavelength (Å)	Star 1–41	Star 1–73	Star 1–87	Star 1–95	Star 1–150	Star 1–229	Star 1–242	Star 1–245	Star 1–267	Star 2–38	Star 2–44	Star 2–52	Star 2–75	Star 2–85
Fe I	6739.52	42	68	38	112	99	93	108	94	110	86	120	118	93	95
Fe I	6750.16	117	143	109	168	157	153	175	157	170	121	...	...	145	171
Fe I	6820.37	...	40	28	91	66	71	82	...	82	64	83	90	69	83
Fe I	6828.60	30	47	38	93	78	90	90	79	102	75	106	110	76	102
Fe I	6839.84	51	79	60	127	97	107	125	94	119	91	123	122	104	126
Fe I	6841.34	38	55	54	105	...	101	101	105	...	96	103	99	95	109
Fe I	6842.69	22	34	29	75	62	64	74	70	81	59	66	73	75	80
Fe I	6851.65	21	37	18	82	63	69	78	62	85	59	76	89	75	78
Fe I	6855.72	...	32	21	70	37	57	44	44	75	43	48	82	45	65
Fe I	6858.16	26	43	33	84	69	78	73	82	93	73	72	78	85	92
Fe I	6898.31	...	16	...	48	47	41	56	...	55	41	63	65	50	61
Fe I	6960.33	...	17	8	33	28	26	45	...	52	...	32	62	36	52
Fe I	6978.86	124	143	120	179	156	169	170	145	155	163	...	...	155	195
Fe I	6988.53	63	84	62	118	110	110	125	98	120	104	115	131	111	122
Fe I	7007.98	...	40	16	74	61	60	75	59	75	62	89	88	65	86
Fe I	7022.96	57	72	58	105	97	103	110	99	135	92	119	115	102	121
Fe I	7024.64	29	...	32	...	...	73	...	97	126	91	107	...	89	105
Fe I	7038.22	47	74	53	125	92	98	117	90	116	83	98	120	103	106
Fe I	7090.39	45	85	52	124	97	104	125	106	109	91	132	145	104	125
Fe I	7127.57	...	...	...	...	36	42	73	...	...	38	...	...	53	...
Fe I	7130.93	68	117	73	155	123	120	148	129	132	105	134	...	135	147
Fe I	7132.99	29	49	37	89	74	73	98	80	91	70	90	124	86	86
Fe I	7142.52	...	43	...	84	48	53	69	53	...	45	56	...	57	76
Fe I	7145.31	...	...	22	63	66	68	96	87	86	63	94	...	82	...
Fe I	7151.46	43	85	46	101	88	99	119	83	105	87	94	119	98	115
Fe I	7180.00	80	89	65	139	122	125	154	123	130	108	132	...	123	143
Fe I	7256.14	...	...	...	...	22	33	29	...	53	29	35	47	33	36
Fe I	7396.53	...	13	...	28	15	29	33	28	41	24	21	38	28	37
Fe I	7411.16	...	124	94	157	133	137	156	136	154	135	148	...	148	159
Fe I	7418.67	...	58	41	...	78	84	95	78	90	84	94	97	85	97
Fe I	7421.56	...	14	...	53	32	43	41	31	52	32	38	45	39	52
Fe I	7445.76	...	136	114	175	151	173	182	169	182	153	...	...	166	180
Fe I	7454.00	...	32	11	43	31	39	40	...	59	37	38	67	39	62
Fe I	7461.53	47	78	50	117	91	91	112	...	112	93	125	121	106	110
Fe II	5414.07	...	21	26	32	24	35	35	43	38	29	38	...	24	49
Fe II	5425.26	26	38	35	41	42	48	46	55	36	42	57	40	48	53
Fe II	6149.26	32	30	35	35	32	40	33	53	45	34	37	58	43	62
Fe II	6247.55	38	41	39	50	49	56	67	54	61	56	48	43	47	53
Fe II	6369.46	16	22	...	31	27	37	26	30	24	...	30	21	...	...
Fe II	6456.39	48	57	54	59	58	66	67	75	61	66	58	58	51	73
Fe II	6516.08	53	43	...	68	64	68	72	95:	50	76	72	73	71	71
Y II	5289.82	≤14:	27	...	41	27:	27:	27	...	43	21	33:	78	31	57
Y II	5728.89	17	...	...	24	13	15	14	...	31	19	36	53	19	35
La II	5808.31	...	19	11	71	33	27	43	...	52:	44	61	102	46	55
La II	6262.29	...	89	...	156	93	97	145	98	194	87	...	...	154	195

Table 3—Continued

Ion	Wavelength (Å)	Star 1–41	Star 1–73	Star 1–87	Star 1–95	Star 1–150	Star 1–229	Star 1–242	Star 1–245	Star 1–267	Star 2–38	Star 2–44	Star 2–52	Star 2–75	Star 2–85
La II	6390.48	20	59	23	92	64	62	81	60	111	64	92	132	67	91
La II	6526.98	26	49	19	167	124	119	162	73	190	72	175	230	127	156
La II	6774.27	25	54	25	103	70	59	99	76	126	85	100	195	96	115
Eu II	6645.13	31	45	37	60	61	58	60	47	68	61	76	77	65	62

Table 4. Absorption Line Parameters

Ion	Wavelength (Å)	EP (eV)	log gf	Reference
Na I	5682.65	2.100	−0.700	q
Na I	6154.23	2.100	−1.570	r
Na I	6160.75	2.100	−1.270	r
Al I	5557.07	3.140	−2.110	p
Al I	6696.03	3.140	−1.481	p
Al I	6698.67	3.140	−1.782	p
Si I	5690.43	4.930	−1.75	tq
Si I	6237.33	5.610	−1.01	t
Si I	6721.84	5.860	−1.17	t
Si I	6976.50	5.950	−1.04	t
Si I	7235.33	5.610	−1.46	t
Si I	7405.79	5.610	−0.66	t
Si I	7415.96	5.610	−0.73	t
Si I	7423.51	5.620	−0.58	t
Ca I	5260.39	2.520	−1.719	j
Ca I	5581.98	2.520	−0.555	j
Ca I	5588.76	2.520	+0.358	j
Ca I	5590.13	2.520	−0.571	j
Ca I	5867.57	2.930	−1.64	t
Ca I	6156.02	2.520	−2.49	t
Ca I	6161.30	2.520	−1.266	j
Ca I	6166.44	2.520	−1.142	j
Ca I	6169.04	2.520	−0.797	j
Ca I	6169.56	2.520	−0.478	j
Ca I	6449.82	2.520	−0.502	j
Ca I	6455.61	2.520	−1.290	j
Ca I	6471.67	2.520	−0.686	j
Ca I	6493.79	2.520	−0.109	j
Ca I	6508.85	2.520	−2.50	t
Ca I	6572.80	0.000	−4.31	t
Ca I	7148.15	2.710	+0.137	j
Ca I	7326.16	2.930	−0.23	t
Ti I	5223.63	2.092	−0.558	i
Ti I	5282.40	1.053	−1.300	i
Ti I	5295.78	1.066	−1.633	i
Ti I	5384.63	0.826	−2.910	i
Ti I	5436.70	0.899	−2.500	i
Ti I	5453.65	1.443	−1.610	i
Ti I	5471.21	1.443	−1.400	i
Ti I	5474.23	1.460	−1.230	i
Ti I	5503.90	2.578	+0.020	i
Ti I	5648.57	2.495	−0.260	i
Ti I	6743.13	0.900	−1.630	i
Ti I	6861.45	2.270	−0.740	i

Table 4—Continued

Ion	Wavelength (Å)	EP (eV)	log gf	Reference
Ti I	7251.72	1.430	−0.770	i
Ti II	5226.55	1.570	−1.300	i
Ti II	5336.78	1.582	−1.700	i
Ti II	6606.98	2.060	−2.790	i
Fe I	6151.62	2.180	−3.310	adfgA
Fe I	6173.34	2.220	−2.863	dfg
Fe I	6180.21	2.730	−2.615	abfgA
Fe I	6188.00	3.940	−1.673	fg
Fe I	6219.29	2.200	−2.426	adgA
Fe I	6229.23	2.830	−2.821	bfg
Fe I	6240.65	2.220	−3.212	abfg
Fe I	6246.33	3.600	−0.796	abg
Fe I	6270.23	2.860	−2.543	abfg
Fe I	6271.28	3.320	−2.719	fgA
Fe I	6298.00	2.220	−2.681	adfgA
Fe I	6335.34	2.200	−2.175	ag
Fe I	6336.83	3.690	−0.840	gA
Fe I	6353.85	0.910	−6.35	t
Fe I	6355.04	2.840	−2.332	abfA
Fe I	6380.75	4.190	−1.366	afg
Fe I	6392.54	2.280	−3.957	g
Fe I	6393.61	2.430	−1.505	abg
Fe I	6411.66	3.650	−0.646	abg
Fe I	6475.63	2.560	−2.929	afg
Fe I	6481.88	2.280	−2.980	adfgA
Fe I	6494.99	2.400	−1.246	adg
Fe I	6498.95	0.960	−4.675	aefg
Fe I	6518.37	2.830	−2.406	abfgA
Fe I	6591.31	4.590	−1.997	g
Fe I	6593.87	2.430	−2.377	adfg
Fe I	6597.57	4.770	−0.970	f
Fe I	6608.04	2.270	−3.939	fg
Fe I	6627.56	4.530	−1.559	fg
Fe I	6646.97	2.600	−3.917	g
Fe I	6648.12	1.010	−5.72	t
Fe I	6699.14	4.590	−2.106	gA
Fe I	6703.58	2.760	−3.059	fg
Fe I	6704.50	4.200	−2.587	g
Fe I	6705.11	4.610	−1.05	t
Fe I	6710.32	1.480	−4.807	g
Fe I	6713.75	4.790	−1.479	fg
Fe I	6715.39	4.590	−1.540	f
Fe I	6716.25	4.560	−1.847	g
Fe I	6725.36	4.100	−2.227	g
Fe I	6726.67	4.590	−1.087	g
Fe I	6733.15	4.620	−1.479	fg

Table 4—Continued

Ion	Wavelength (Å)	EP (eV)	log gf	Reference
Fe I	6739.52	1.560	−4.801	bg
Fe I	6750.16	2.420	−2.592	abdf
Fe I	6820.37	4.620	−1.214	fg
Fe I	6828.60	4.640	−0.843	fg
Fe I	6839.84	2.560	−3.378	fg
Fe I	6841.34	4.610	−0.733	fg
Fe I	6842.69	4.640	−1.224	fg
Fe I	6851.65	1.600	−5.247	g
Fe I	6855.72	4.390	−1.747	g
Fe I	6858.16	4.590	−0.939	afg
Fe I	6898.31	4.220	−2.157	g
Fe I	6960.33	4.570	−1.907	g
Fe I	6978.86	2.480	−2.465	abdg
Fe I	6988.53	2.400	−3.519	fg
Fe I	7007.98	4.180	−1.929	fg
Fe I	7022.96	4.190	−1.148	fg
Fe I	7024.64	4.540	−1.106	afg
Fe I	7038.22	4.220	−1.214	fg
Fe I	7090.39	4.230	−1.109	fg
Fe I	7127.57	4.990	−1.177	g
Fe I	7130.93	4.300	−0.708	fg
Fe I	7132.99	4.060	−1.635	afg
Fe I	7142.52	4.930	−1.017	g
Fe I	7145.31	4.610	−1.23	t
Fe I	7151.46	2.480	−3.657	g
Fe I	7180.00	1.480	−4.707	g
Fe I	7256.14	4.930	−1.517	g
Fe I	7396.53	4.990	−1.567	g
Fe I	7411.16	4.280	−0.287	g
Fe I	7418.67	4.140	−1.388	ag
Fe I	7421.56	4.640	−1.727	g
Fe I	7445.76	4.260	+0.053	g
Fe I	7454.00	4.190	−2.337	g
Fe I	7461.53	2.560	−3.507	g
Fe II	5414.07	3.221	−3.79	h
Fe II	5425.26	3.199	−3.36	h
Fe II	6149.26	3.889	−2.724	B
Fe II	6247.55	3.892	−2.38	lt
Fe II	6369.46	2.891	−4.253	B
Fe II	6456.39	3.900	−2.13	lt
Fe II	6516.08	2.891	−3.42	klt
Y II	5289.82	1.030	−1.85	o
Y II	5402.77	1.840	−0.52	t
Y II	5728.89	1.840	−1.12	o
La II	5808.31	0.000	−2.20	C

Table 4—Continued

Ion	Wavelength (Å)	EP (eV)	log gf	Reference
La II	6262.29	0.403	−1.22	D
La II	6390.48	0.320	−1.41	Du
La II	6526.98	0.235	−1.74	C
La II	6774.27	0.130	−1.71	u
Eu II	6645.13	1.380	+0.12	E

References. —
1. Reference codes are the same as McWilliam & Rich (1994; MR94), with the addition of six new sources: (A) Bard & Kock 1994; (B) Kurucz 1988; (C) Arnesen 1977; (D) Lawler et al 2001a; (E) Lawler et al 2001b.
2. Solar gf values for Fe I were increased by 0.01 dex from MR94, to account for a reduced assumed solar iron abundance.

Table 5. Spectroscopic and Photometric Temperatures

Star	$T_{ion.}$ (°K)	$T_{ex.}$ (°K)	ΔT(ex−ion) (°K)	$T_{phot.}$ (°K)	ΔT(ion−phot) (°K)
1–41	4220	4176	−44	4030	190
1–73	4160	4269	109	4038	122
1–87	4430	4341	−89	4165	265
1–95	4120	4293	173	3975	145
1–150	4180	4207	27	4025	155
1–229	4420	4316	−104	4151	269
1–242	4260	4282	22	3925	335
1–245	4550	4443	−107	3988	562
1–267	4190	4264	74	3977	213
2–38	4360	4491	131	4116	244
2–44	4230	4253	23	3902	328
2–52	4130	4256	126	3855	275
2-75	4250	4353	103	4031	219
2-85	4420	4443	23	4259	161

Table 6. Adopted Stellar Parameters

Star	B.C. (mag)	M_{bol} (mag)	T_{eff} (°K)	log g	[A/H]	ξ (km/s)	t (Gyr)	σ_t (Gyr)
1–41	−0.88	−3.28	4220	0.6	−1.60	2.07	12.5	5.0
1–73	−0.91	−3.01	4160	0.8	−1.10	1.66	4.1	4.7
1–87	−0.68	−2.59	4430	1.1	−1.25	1.73	2.8	2.1
1–95	−0.96	−2.80	4120	1.0	−0.35	1.81	1.0	0.3
1–150	−0.88	−2.36	4180	1.1	−0.60	1.63	2.8	2.3
1–229	−0.61	−1.82	4420	1.6	−0.35	1.64	1.0	0.3
1–242	−0.81	−1.90	4260	1.5	−0.30	1.98	1.2	0.4
1–245	−0.59	−1.67	4550	1.7	−0.35	1.78	0.8	0.3
1–267	−0.89	−1.86	4190	1.5	−0.05	1.58	1.2	0.2
2–38	−0.73	−2.31	4360	1.4	−0.40	1.38	0.8	0.4
2–44	−0.84	−2.28	4230	1.3	−0.40	1.99	1.2	0.2
2–52	−0.96	−2.27	4130	1.3	−0.05	1.68	0.8	0.5
2-75	−0.82	−1.75	4250	1.5	−0.30	1.56	1.6	0.8
2-85	−0.70	−1.46	4420	1.8	+0.00	1.60	0.5	0.4

Table 7. Chemical Abundances

Star	[Fe/H]	$[Fe/H]_{eff}$	[Si/Fe]	[Ca/Fe]	[Ti/Fe]	[α/Fe][a]	[Na/Fe]	[Al/Fe]	[Y/Fe]	[La/Fe]	[Eu/Fe]
1–41	−1.58	−1.35	+0.32	+0.31	+0.33	+0.32	−0.20	+0.19	$\lesssim$ +0.17	+0.06	+0.48
1–73	−1.09	−0.91	+0.44	+0.20	+0.11	+0.25	+0.22	+1.12	−0.05	+0.18	+0.54
1–87	−1.27	−1.09	+0.13	+0.30	+0.32	+0.25	−0.11	...	−0.06	+0.11	+0.60
1–95	−0.34	−0.34	+0.07	−0.14	+0.08	0.00	−0.38	−0.35	−0.06	+0.42	+0.35
1–150	−0.61	−0.62	+0.01	+0.01	−0.05	−0.01	−0.43	−0.31	−0.14	+0.32	+0.62
1–229	−0.36	−0.36	0.00	−0.04	+0.05	0.00	−0.53	−0.41	−0.11	+0.40	+0.59
1–242	−0.31	−0.32	0.00	−0.08	+0.03	−0.02	−0.34	−0.31	−0.10	+0.39	+0.50
1–245	−0.35	−0.32	−0.06	+0.13	+0.09	+0.05	−0.36	+0.02	−0.14	+0.40	+0.41
1–267	−0.07	−0.07	+0.08	−0.07	0.00	0.00	−0.43	−0.38	+0.12	+0.56	+0.55
2–38	−0.42	−0.42	−0.06	+0.08	−0.02	0.00	−0.67	−0.34	−0.07	+0.35	+0.66
2–44	−0.39	−0.32	−0.08	+0.12	+0.22	+0.09	−0.13	−0.15	+0.12	+0.43	+0.70
2–52	−0.06	−0.01	−0.07	+0.05	+0.22	+0.07	−0.24	−0.36	+0.49	+0.96	+0.59
2–75	−0.31	−0.29	+0.01	0.00	+0.08	+0.03	−0.36	−0.26	−0.02	+0.47	+0.66
2–85	+0.03	0.00	−0.05	−0.04	−0.02	−0.04	−0.39	−0.42	+0.20	+0.55	+0.49
1–σ error	0.05	0.05	0.07	0.07	0.07	0.07	0.11	0.10	0.18	0.08	0.13
Metal Poor Average	−1.31	−1.12	+0.30	+0.27	+0.25	+0.27	−0.16[b]	+0.19[b]	+0.17	+0.12	+0.54
Standard Deviation	0.25	0.22	0.16	0.06	0.12	0.04	0.06	...	0.12	0.06	0.06
Metal Rich Median	−0.34	−0.32	0.00	0.00	+0.05	0.00	−0.38	−0.34	−0.04	+0.42	+0.59
Standard Deviation	0.19	0.19	0.06	0.09	0.09	0.05	0.14	0.14	0.24	0.19	0.12

[a][α/Fe] is the average of the Si, Ca and Ti ratios.

[b]The star 1–73 has been omitted from the calculation of the average element ratio for the metal–poor stars because its Na and Al abundance has been elevated over primordial because of proton-burning.